



ANALYSIS OF THE APPLICATION OF A TRIGGERED ISOMER
HEAT EXCHANGER AS A REPLACEMENT FOR THE
COMBUSTION CHAMBER IN AN OFF-THE-SHELF TURBOJET

THESIS

Carl Rex Hartsfield, Captain, USAF

AFIT/GAE/ENY/01M-04

DEPARTMENT OF THE AIR FORCE
AIR UNIVERSITY

AIR FORCE INSTITUTE OF TECHNOLOGY

Wright-Patterson Air Force Base, Ohio

APPROVED FOR PUBLIC RELEASE; DISTRIBUTION UNLIMITED

20010523 011

The views expressed in this thesis are those of the author and do not reflect the official policy or position of the United States Air Force, Department of Defense or the United States Government.

AFIT/GAE/ENY/01M-04

ANALYSIS OF THE APPLICATION OF A TRIGGERED ISOMER
HEAT EXCHANGER AS A REPLACEMENT FOR THE
COMBUSTION CHAMBER IN AN OFF-THE-SHELF TURBOJET

THESIS

Presented to the Faculty

Department of Aeronautical and Astronautical Engineering

School of Engineering and Management

Air Force Institute of Technology

Air University

Air Education and Training Command

In Partial Fulfillment of the Requirements for the

Degree of Master of Science in Aeronautical Engineering

Carl Rex Hartsfield, B.A.E.

Captain, USAF

March 2001

APPROVED FOR PUBLIC RELEASE; DISTRIBUTION UNLIMITED

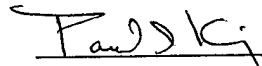
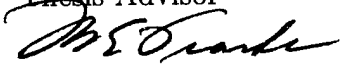

AFIT/GAE/ENY/01M-04

ANALYSIS OF THE APPLICATION OF A TRIGGERED ISOMER
HEAT EXCHANGER AS A REPLACEMENT FOR THE
COMBUSTION CHAMBER IN AN OFF-THE-SHELF TURBOJET

Carl Rex Hartsfield, B.A.E.

Captain, USAF

Approved:

 _____	<u>7 Mar 01</u>
Dr. Paul I. King Thesis Advisor	Date
 _____	<u>7 Mar 2001</u>
Dr. Milton E. Franke Committee Member	Date
 _____	<u>8 Mar 2001</u>
Dr. William C. Elrod Committee Member	Date

Acknowledgements

I would like to thank several people for the time, guidance and attention they afforded either me or this work. My sincere appreciation to my advisors, Dr. Paul King and Dr. Milton Franke, for their guidance and assistance in this research. Their inputs and involvement are a large part of my success. I must extend my deep gratitude to Mr. Jay Anderson and Ms. Leslie Robinson, whose efforts in procuring and setting up the computer hardware I used enabled me to get started quickly and also provided invaluable assistance with correcting computer faults and failures. I thank my colleagues at AFIT, including, but not limited to, Captain Mark Suriano, Captain Patrick Wade, Captain Brian McDonald, Lieutenant William Shipman and Lieutenant Andrew White for adding occasional humor, helping with technical problems, providing insights and generally breaking the tension throughout my tenure at AFIT.

My deepest appreciation and gratitude go to my wife and daughters. They were always there, with encouraging words and a sympathetic ear, and my daughters' smiles and insistence that I play now kept me from driving myself crazy. I thank all three of you from the bottom of my heart-I couldn't have done this without you.

Carl Rex Hartsfield

Table of Contents

	Page
Acknowledgements	iv
List of Figures	viii
List of Tables	x
List of Symbols	xi
List of Abbreviations	xiv
Abstract	xv
I. Introduction	1-1
1.1 Motivation	1-1
1.2 Problem Statement	1-2
1.3 Summary of Current Knowledge	1-3
1.4 Present Work	1-5
1.5 Outline	1-7
II. Background and Theory	2-1
2.1 Navier-Stokes Equations	2-1
2.1.1 Substantial Derivative Operator	2-1
2.1.2 Continuity Equation	2-1
2.1.3 Momentum Equation	2-2
2.1.4 Energy Equation	2-3
2.1.5 Perfect Gas Relationship	2-3
2.2 Turbulence Model	2-4

	Page
2.3 Heat Transfer	2-5
2.3.1 Heat Flow in the Heat Exchanger	2-5
2.3.2 Convection	2-6
2.3.3 Pressure Losses Due to Heating	2-8
2.4 Gas Turbine Performance	2-9
2.4.1 On-Design Gas Turbine Performance	2-9
2.4.2 Off-Design Gas Turbine Performance	2-11
2.5 Triggered Hafnium Decay	2-12
2.6 Radiation Shielding	2-13
III. Computational Setup	3-1
3.1 Hardware	3-1
3.2 Software	3-1
3.3 Software Inputs	3-1
3.3.1 Solver Settings	3-1
3.3.2 Geometry	3-2
3.3.3 Concentric Tubes	3-3
3.3.4 Trapezoidal Fins	3-6
3.3.5 Rectangular Fins	3-6
3.3.6 Radial Fin Inlet and Outlet	3-11
3.3.7 Grid Generation	3-11
3.3.8 Reference Conditions	3-12
3.3.9 Boundary Conditions	3-13
3.3.10 Thermal Boundary Conditions	3-13
3.4 Code Validation	3-17

	Page
IV. Results and Discussion	4-1
4.1 Pressure Ratios and Total Temperature Increases	4-1
4.1.1 Concentric Tube Geometry	4-1
4.1.2 Trapezoidal Radial Fin Geometry	4-7
4.1.3 Rectangular Radial Fin Geometry	4-10
4.2 Heat Exchanger Performance Trends	4-12
4.2.1 Heat Exchanger Mass	4-14
4.3 Engine Performance Estimates	4-16
4.3.1 Static Sea-Level Performance	4-16
4.3.2 Performance at Other Flight Conditions	4-18
4.4 Grid Independence	4-18
V. Conclusions and Recommendations	5-1
5.1 Conclusions	5-1
5.2 Recommendations	5-2
Appendix A. Temperature Corrections for Variable Specific Heats	A-1
Appendix B. Building a Model in ANSYS®	B-1
Bibliography	BIB-1
Vita	VITA-1

List of Figures

Figure	Page
1.1. Basic Configurations of Heat Exchanger	1-4
1.2. Schematic View of J-57 Turbojet	1-6
2.1. Differential Control Volume for Heat Flow Calculations	2-6
2.2. Burner Pressure Ratio and Turbine Inlet Temperature Effects	2-10
3.1. Schematic View of Concentric Tube Geometry	3-4
3.2. 0.5 mm Thick Tubes, Compact Concentric Geometry	3-4
3.3. 2.0 mm Thick Tubes, Compact Concentric Geometry	3-5
3.4. 0.5 mm Thick Staggered Concentric Tubes, Compact Geometry	3-5
3.5. 2.0 mm Thick Tubes, Full-Scale Concentric Geometry	3-6
3.6. Schematic View of Trapezoidal Radial Fin Geometry	3-7
3.7. Schematic View of Two Trapezoidal Fins	3-8
3.8. Example of Radial Fin Computational Geometry	3-8
3.9. Schematic View of Rectangular Radial Fin Geometry	3-9
3.10. Schematic View of Two Rectangular Fins	3-10
3.11. Radial Geometry Inlet	3-11
3.12. Radial Geometry Outlet	3-12
3.13. Variation of Wall Temperature along Fin/Tube Surface	3-14
3.14. Comparison of Dynamic Pressure Distributions	3-17
4.1. Exit Flow Parameters, 0.5 mm Compact Concentric Tubes	4-2
4.2. Heat Flux and Heat Transfer Coefficient Distributions, 0.5 mm Con- centric Tubes	4-3
4.3. Exit Flow Parameters, 2.0 mm Compact Concentric Tubes	4-4
4.4. Exit Flow Parameters, 0.5 mm Staggered Concentric Tubes	4-5

Figure	Page
4.5. Exit Flow Parameters, Full-Scale Concentric Tubes	4-6
4.6. Exit Flow Parameters, Trapezoidal Fins, 41 m/s	4-9
4.7. Exit Flow Parameters, Trapezoidal Fins, 29 m/s	4-9
4.8. Heat Flux and Heat Transfer Coefficient Distribution on Radial Fin .	4-10
4.9. Exit Flow Parameters, Rectangular Fins, 41 m/s	4-11
4.10. Exit Flow Parameters, Rectangular Fins, 29 m/s	4-12
4.11. Fin Spacing Effects on Flow Parameters	4-14
4.12. Effects of Reynolds Number on T_{T4} Available	4-15
4.13. Effects of Altitude on Required and Available T_{T4}	4-19

List of Tables

Table	Page
3.1. Dimensions of Geometries Used in Trapezoidal Fin Computations . .	3-7
3.2. Dimensions of Geometries Used in Rectangular Fin Computations . .	3-9
3.3. Comparison of Temperature Distributions on a Cylinder in Crossflow	3-18
4.1. J-57 Burner Inlet Conditions in Flight	4-7
4.2. Concentric Tube Heat Exchanger Outlet Conditions in Flight	4-7
4.3. Reynolds Number Effects on T_{T4} and π_b	4-14
4.4. Mass and Solid Volume of Heat Exchangers	4-15
4.5. Critical Engine Parameters for the J-57 Turbojet	4-17
4.6. Estimated J-57 Sea Level Static Thrust with Heat Exchangers Installed	4-17

List of Symbols

English Symbols

Symbol	Definition
A	Area (m^2)
CE	Radiation Generation Rate (W)
C_μ	Constant used in turbulence model
$C_{\epsilon 1}$	Constant used in turbulence model
$C_{\epsilon 2}$	Constant used in turbulence model
\dot{D}	Radiation dose rate (Grays/s)
D_h	Hydraulic diameter (m)
F	Uninstalled engine thrust (N)
G	Mass flow rate per unit area ($\frac{kg}{s \cdot m^2}$)
g_0	Acceleration due to gravity ($\frac{m}{s^2}$)
h	Enthalpy per unit mass ($\frac{J}{kg}$)
h_f	Heat transfer coefficient ($\frac{W}{m^2 \cdot s}$)
I	Impulse (N)
k	Turbulent kinetic energy (J) or thermal conductivity ($\frac{J}{m \cdot K}$)
l	Bousinesq mixing length (m)
M	Mach number
\bar{M}	Molar mass ($\frac{kg}{kgmol}$)
\dot{m}	Mass flow rate ($\frac{kg}{s}$)
N_u	Nusselt number ($\frac{hD_h}{k}$)
P	Pressure (Pa)
Q	Radiative heat transfer rate ($\frac{W}{m^2}$)
\vec{q}	Conductive heat transfer rate ($\frac{W}{m^2}$)
\dot{q}	heat transfer rate (W)
\dot{q}''	Heat flux per unit area ($\frac{W}{m^2}$)
R	Specific gas constant ($\frac{J}{kg \cdot K}$)

Symbol	Definition
Re	Reynolds number ($\frac{\rho VL}{\mu}$)(L any characteristic length)
R_u	Universal gas constant ($\frac{J}{kgmolK}$)
r	Radius (m)
r_i	Inner radius of an annulus (m)
r_o	Outer radius of an annulus (m)
T	Temperature (K)
T_{T4}	Turbine inlet temperature (K)
t	Time (s)
U_i	Mean velocity in the i direction ($\frac{m}{s}$)
u_i	Fluctuating velocity in the i direction ($\frac{m}{s}$)
u	Velocity in the x-direction
\vec{V}	Velocity vector in two or more dimensions ($\frac{m}{s}$)
v	Velocity in the y-direction ($\frac{m}{s}$)
w	Velocity in the z-direction ($\frac{m}{s}$)
x	Streamwise or Axial direction
y	Direction normal to stream or axis
y^+	Distance from a surface in non-dimensional wall units
z	Direction normal to stream or axis and y-direction

Greek Symbols

Symbol	Definition
γ	Ratio of specific heats ($\frac{c_p}{c_v}$)
γ_c	Ratio of specific heats at low temperatures
γ_h	Ratio of specific heats at high temperatures
ϵ	Turbulent energy dissipation (J)
η_{ch}	High pressure compressor polytropic efficiency
η_{cl}	Low pressure compressor polytropic efficiency
η_{mh}	High pressure spool mechanical efficiency

Symbol	Definition
η_{ml}	Low pressure spool mechanical efficiency
η_t	Turbine polytropic efficiency (both high and low pressure)
μ	Absolute viscosity ($\frac{kg}{ms}$)
μ_t	Turbulent viscosity ($\frac{kg}{ms}$)
ν	Kinematic Viscosity ($\frac{\mu}{\rho}$)($\frac{m^2}{s}$)
ν_t	Turbulent kinematic Viscosity ($\frac{\mu_t}{\rho}$)($\frac{m^2}{s}$)
π_b	Pressure ratio across burner in a gas turbine engine
π_{ch}	Pressure ratio across high pressure compressor
π_{cl}	Pressure ratio across low pressure compressor
$\pi_{D_{max}}$	Maximum diffuser pressure ratio
$\pi_{N_{max}}$	Maximum nozzle pressure ratio
ρ	Density ($\frac{kg}{m^3}$)
σ_ϵ	Constant used in turbulence model
σ_k	Constant used in turbulence model

List of Abbreviations

Abbreviation	Definition
AFIT	Air Force Institute of Technology
ANP	Aircraft Nuclear Propulsion
NEPA	Nuclear Propulsion of Aircraft
PC	Personal Computer

Abstract

The objective of this research was to determine the feasibility of using a nuclear reaction heat source, such as the electromagnetically triggered decay of an isomer, in a solid-state heat exchanger to power an off-the-shelf gas turbine engine. Two primary performance measures examined were the total pressure decrement across the heat exchanger and the total temperature capability leaving the heat exchanger.

The analysis included the use of a commercial software package, ANSYS® 5.6.1, running on a 700 MHz Pentium® III PC. This package includes the FLOTRAN® computational fluid dynamics program, a finite element program based on unstructured meshes, with multiple discretization schemes, turbulence models, and advection options. Boundary conditions on velocity, pressure, temperature, heat flux, and heat generation are available and were used in this research.

Three basic geometries of heat exchanger were explored in this research: concentric annular tubes, radial trapezoidal fins, and a dual, concentric annulus of rectangular fins. These were selected due to the simplicity of geometry and potential ease of manufacture. In addition, because the flow through all of these geometries could be reasonably approximated by a series of two-dimensional flow fields, run times were on the order of 1 day, a significant reduction from 3-D flow calculations.

All three configurations produced sufficient heat transfer. Pressure ratios across the heat exchangers varied in the range from 94.5% to 97.5%. Turbine inlet temperatures varied from 986 K to 1150 K (1775°R to 2070°R). In the J-57 engine, these conditions will produce a static, sea-level thrust of approximately 37,000 N (8,300 lb.) to 47,000 N (10,600 lb.), compared to 46,000 N (10,300 lb.) for the conventional engine.

ANALYSIS OF THE APPLICATION OF A TRIGGERED ISOMER HEAT EXCHANGER AS A REPLACEMENT FOR THE COMBUSTION CHAMBER IN AN OFF-THE-SHELF TURBOJET

I. Introduction

1.1 Motivation

Since 1942, with the creation of the first fission chain reactor, scientists and engineers have contemplated the use of atomic energy to power aerospace vehicles. These proposals began with the idea of flowing light fluids through a nuclear reactor to power a rocket motor. Starting in 1946, and continuing through the 1950s and 1960s, the United States Air Force and the Atomic Energy Commission worked on projects including Nuclear Propulsion of Aircraft (NEPA) and later, Aircraft Nuclear Propulsion (ANP), which explored the use of nuclear reactors to power jet aircraft. Ultimately, these projects were cancelled due to a technical inability to produce a safe, controllable reactor that met the power requirements of flight at a sufficiently low weight, as well as safety concerns for the crew and civilians who might be affected (1:1-6)

Recent developments in controlling the decay of several long half-life isomers of hafnium, lutetium, and tantalum, may have opened another possibility. Some of these isomers have extremely high internal energy states, and an atomic structure which inhibits rapid decay to lower energy states. By triggering rapid decay of these isomers through X-ray bombardment, a controllable release of the internal atomic energy available may be possible. The specific isomer of interest for this study was the 4-quasiparticle isomer of hafnium, which has a half-life of 31 years and an excitation energy of 2.446 mega-electron volts (MeV). This has the potential to release up to

1.3 gigajoules per gram, mostly in the form of heat and some gamma rays. This could represent an extremely compact, controllable heat source with the potential to power an aircraft engine at a fuel consumption rate on the order of ten pounds per day (2:695;3:1). This power source may represent a practical method of achieving extraordinary endurance, free of many of the safety and environmental issues which plagued fission-powered flight programs in the past.

Practical applications of this type of power source could be widespread, depending on the expense and shielding requirements, but long-endurance, unmanned aircraft are one of the first obvious applications. If the expense can be reduced sufficiently, this power source could be practical for any application where long endurance is a desirable characteristic. In any application, the additional weight of radiation shielding over any sensitive components of the aircraft (including personnel) would have to be taken into account.

1.2 Problem Statement

The goal of this study was to determine if a solid-state heat exchanger configuration could be devised that could feasibly replace the combustion chamber in an off-the-shelf gas turbine engine. Solid-state is taken to mean a heat exchanger that does not rely on a fluid for the heat source. Thus, the heat exchanger will generate its own heat, rather than transferring heat from a hot fluid to a cool fluid. For the heat exchanger to be feasible, it must meet several requirements. First, the flow through the heat exchanger must reach stagnation temperatures sufficient to produce thrust. Second, the stagnation pressure losses through the heat exchanger must be low enough to allow operation of the engine. In addition, the added weight of the heat exchanger and the necessary radiation shielding around sensitive areas must not be so high as to require extensive re-design of the airframe to accommodate the engine. Last, the heat exchanger should fit within the existing engine envelope without requiring extensive mechanical changes to the engine systems such as the

drive spools for the compressor stages. To some extent, all of these criteria are application driven. The temperature gain and pressure loss must provide adequate thrust, but exactly what level of thrust is adequate is driven by the intended application, including airframe design and mission. Therefore, for now, it was decided to address the adequacy of the thrust level only as a percentage of the original design thrust of the chosen gas turbine engine (4). It was decided to address the weight issues only in general terms, as they will be driven almost entirely by the precise application. For example, how much radiation shielding is required will depend heavily on the airframe geometry and the amount of radiation that the most sensitive components can tolerate, while the additional weight of the heat exchanger will depend on factors including (but not limited too): the air loads on the fins, the design mission of the aircraft and engine, the turbine inlet temperature required, and the mass flow of air through the heat exchanger.

1.3 Summary of Current Knowledge

Current knowledge in this type of heat exchanger can be divided into two basic areas: work done in the past with aircraft and rockets to be powered by fission reactions, and work done with more conventional heat exchangers and augmenting the heat transfer.

Most work with nuclear powered aircraft was accomplished in the 1950s and 1960s, and concentrated on two concepts. Both used fission reactors, but differed in the mechanism used to heat the air. One was a direct cycle, in which the air was passed directly through the reactor core, located in the engine. The second was an indirect cycle, in which the reactor heated a liquid metal, which was circulated to a liquid-to-air heat exchanger in the engine (1:3).

Of these two, the first was most directly applicable to the current work, as it involves solid-state heat exchangers, without tubes to significantly disturb the airflow. Various simple configurations were explored, in terms of advantages and disadvantage

in the fission reactor application. These included flat plates, solid rods, and tubes. These are shown schematically in Figure 1.1. Flat plates hold the advantages of ease of manufacture, easy structural support and a near immunity to blocked passages. Debris and uneven fuel loading will not drastically affect the flow in a channel, as the flow will simply go around the area. Solid rods have similar advantages to plates, except that structural support is significantly more complicated, and non-uniform distribution of heat-generating material can lead to significant temperature gradients. Drilling holes in a solid block, or stacking interlocking cylinders would lead to the tube configuration. This is the most structurally stable configuration, however, it is also the most subject to blocking and failure due to local hot spots (1:152;5;6). Except for the difference in materials (uranium instead of hafnium) and the concurrent difference in energy content, this is a close analog of the problem at hand. In the interest of simplicity of manufacturing and support, all of the heat exchanger configurations used in this research were variations on the flat plate configuration.

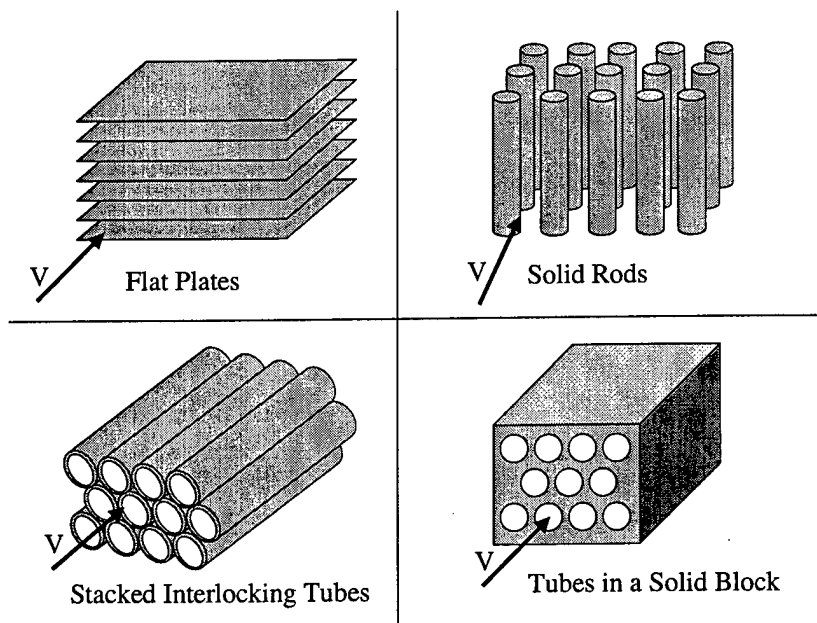


Figure 1.1 Basic Configurations of Heat Exchanger

For the purposes of this study, the second method of transferring heat to the air from the nuclear reactor overlaps with the research on conventional heat exchangers. In both cases, heat is transferred from a liquid traveling in tubes through fins attached to the tubes, the difference being in the nature of the liquid, with the reactor using liquid metals, such as sodium. The aim with most heat exchangers of this type is to cool the liquid, rather than heat the air, leading to less attention being paid to the efficiency of the air side of the heat exchanger, at least with respect to pressure losses. Much of the effort in increasing heat transfer is in various methods of augmenting the heat transfer, usually by inducing turbulence. Devices such as ribbed fins, interrupted fins, and roughened surfaces are used to create turbulence and higher heat transfer to the air at the cost of reduced total pressure across the heat exchanger. In the liquid side of the liquid-air heat exchanger, twisted ribbons and similar devices can be used to increase the heat transfer from the liquid (also by inducing additional turbulence). In some heat exchangers, multiple passes for one or both fluids are used to increase the heat transfer from a given volume of fluid (7;8;9:417-477;10).

There are also active methods for augmenting heat transfer, including vibration of the surfaces of fluids, electrostatic fields, and suction or injection jets onto the surfaces, but these would add significant weight to an already hefty gas turbine engine and hafnium heat exchanger combination (7).

1.4 Present Work

The present work used the geometry and combustion chamber inlet conditions of the J-57 turbojet, used in the Boeing 707, KC-135 and some models of B-52. This engine was chosen largely for its simple geometry and the availability of pressure, temperature, and geometric data. This engine is shown schematically in Figure 1.2. As shown in the figure, heat exchangers (manufactured from hafnium isomer) would be installed in place of the combustion chamber. All of the heated

surfaces of these heat exchangers were assumed to be made of the hafnium isomer. Therefore, the heat exchanger itself was also the heat source. Simulations using ANSYS®/FLOTRANTM (version 5.6.1) (11), on a Pentium® III platform, were run to evaluate the effectiveness of several heat exchanger configurations in transferring sufficient heat to the airflow with low pressure loss. These heat exchanger configurations were designed under the assumption that the isomer heat source would make up the heated surfaces of the heat exchanger. Since this was only a feasibility study, very little has been done to optimize the configurations, or attempt to exceed the performance of the original engine.

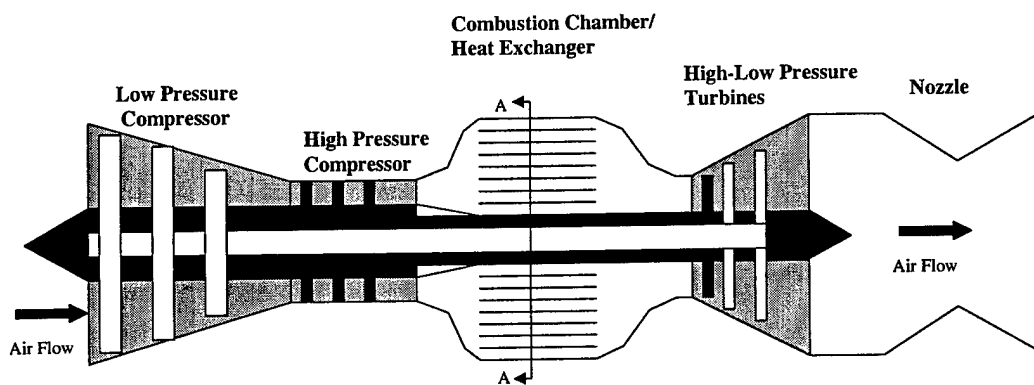


Figure 1.2 Schematic View of J-57 Turbojet

1.5 Outline

This section contains an overview of the chapters to follow. Chapter 2 contains a discussion of the theory and equations which pertain to the current work. Discussion of the methods, hardware, and software, including inputs to the software (geometries, grids, and boundary conditions) used in this work follows in Chapter 3. The results of computation are presented in Chapter 4, including some estimates of performance relative to the baseline (petroleum powered) engine. Conclusions and recommendations for future research in this area are contained in Chapter 5.

II. Background and Theory

This chapter contains a discussion of the Navier-Stokes equations for fluid flow, heat transfer, and the turbulence model used in the computation, as well as background information on the process of triggered hafnium decay and estimating the radiation shielding requirements.

2.1 Navier-Stokes Equations

The program used in this research, ANSYS® (11), implements the Navier-Stokes equations through a finite-element method of approximating differentials. To understand the operation of this program, it is necessary to understand the basic equations on which it is built. Therefore, this section includes a basic presentation and explanation of the Navier-Stokes equations.

2.1.1 Substantial Derivative Operator. Before beginning a presentation of the Navier-Stokes equations, it is imperative that the reader understand the $\frac{D()}{Dt}$ operator for the substantial derivative. This allows a much more compact presentation of the equations than would otherwise be possible. The $\frac{D()}{Dt}$ operator can be defined as (12:61-73;13):

$$\frac{D()}{Dt} = \frac{\partial()}{\partial t} + u \frac{\partial()}{\partial x} + v \frac{\partial()}{\partial y} + w \frac{\partial()}{\partial z} \quad (2.1)$$

and will be used repeatedly in this presentation.

2.1.2 Continuity Equation. If the conservation of mass law is applied to a fluid passing through an infinitesimal, fixed control volume, the continuity equation can be derived:

$$\frac{\partial \rho}{\partial t} + \nabla \cdot (\rho \vec{V}) = 0 \quad (2.2)$$

where ρ is the fluid density and \vec{V} is the vector fluid velocity. The first term represents the rate of change of density in the control volume, and the second term

represents the rate of mass flow out of the control volume per unit volume (12:61-73;14:3-6;15:250). This can be further reduced in some cases to eliminate changes in density, but not in this case. Since the problem was steady state, it would seem that the time derivative term could have been dropped, but this was not the case. The nature of the equation set is such that the problem is more easily addressed in a transient sense, where finite time derivatives are allowed. In a steady-state problem, this equation set is elliptic, where conditions at any location affect conditions at all locations. This is computationally more difficult. By making the problem transient, the equation set is hyperbolic, and computationally easier (13).

2.1.3 Momentum Equation. By applying Newton's second law to a similar control volume, and simplifying the result using the continuity equation (Equation 2.2), the following momentum equations can be derived (in the x, y, and z directions, respectively):

$$\begin{aligned}
 \rho \frac{Du}{Dt} &= \rho f_x - \frac{\partial p}{\partial x} + \frac{\partial}{\partial x} \left[\frac{2}{3} \mu \left(2 \frac{\partial u}{\partial x} - \frac{\partial v}{\partial y} - \frac{\partial w}{\partial z} \right) \right] + \frac{\partial}{\partial y} \left[\mu \left(\frac{\partial u}{\partial y} + \frac{\partial v}{\partial x} \right) \right] \\
 &\quad + \frac{\partial}{\partial z} \left[\mu \left(\frac{\partial w}{\partial x} + \frac{\partial u}{\partial z} \right) \right] \\
 \rho \frac{Dv}{Dt} &= \rho f_y - \frac{\partial p}{\partial y} + \frac{\partial}{\partial x} \left[\mu \left(\frac{\partial v}{\partial x} + \frac{\partial u}{\partial x} \right) \right] + \frac{\partial}{\partial y} \left[\frac{2}{3} \mu \left(2 \frac{\partial v}{\partial y} - \frac{\partial u}{\partial x} - \frac{\partial w}{\partial z} \right) \right] \\
 &\quad + \frac{\partial}{\partial z} \left[\mu \left(\frac{\partial v}{\partial z} + \frac{\partial w}{\partial y} \right) \right] \\
 \rho \frac{Dw}{Dt} &= \rho f_z - \frac{\partial p}{\partial z} + \frac{\partial}{\partial x} \left[\mu \left(\frac{\partial w}{\partial x} + \frac{\partial u}{\partial z} \right) \right] + \frac{\partial}{\partial y} \left[\mu \left(\frac{\partial v}{\partial z} + \frac{\partial w}{\partial y} \right) \right] \\
 &\quad + \frac{\partial}{\partial z} \left[\frac{2}{3} \mu \left(2 \frac{\partial w}{\partial z} - \frac{\partial u}{\partial x} - \frac{\partial v}{\partial y} \right) \right]
 \end{aligned} \tag{2.3}$$

where f_x , f_y , and f_z are the body forces in the x, y, and z directions, μ is the absolute viscosity, and u, v, and w are the components of velocity in the x, y, and z directions. This formulation ignores bulk viscosity and assumes that we have a Newtonian fluid. For the purposes of the problem covered here, body forces were neglected, as the problem is largely at a single altitude, and the only body force expected would have

been gravity. Again, the problem was treated as transient, and μ was left inside the differential, since large temperature changes are expected, and viscosity is a function of temperature (12:61-73;14:3-6;15:253)

2.1.4 Energy Equation. By applying the First Law of Thermodynamics to the fluid passing through the same control volume, and neglecting shaft work, the following energy equation was found:

$$\rho \frac{Dh}{Dt} - \frac{DP}{Dt} = \frac{\partial Q}{\partial t} - \nabla \cdot \vec{q} + \mu \left[2 \left(\frac{\partial u}{\partial x} \right)^2 + 2 \left(\frac{\partial v}{\partial y} \right)^2 + 2 \left(\frac{\partial w}{\partial z} \right)^2 - \frac{2}{3} \left(\nabla \cdot \vec{V} \right)^2 + \left(\frac{\partial u}{\partial y} + \frac{\partial v}{\partial x} \right)^2 + \left(\frac{\partial u}{\partial z} + \frac{\partial w}{\partial x} \right)^2 + \left(\frac{\partial v}{\partial z} + \frac{\partial w}{\partial y} \right)^2 \right] \quad (2.4)$$

where h is enthalpy, P is pressure, Q is radiative heat transfer, \vec{q} is conductive heat transfer, and the terms in brackets make up the viscous dissipation element (12:61-73;14:3-6;15:257). The challenge at this point, for this research was to define the \vec{q} . Q is neglected and, once again, the transient terms are kept for computational purposes.

2.1.5 Perfect Gas Relationship. To make a complete equation set of the Navier-Stokes relations (Equations 2.2, 2.3, and 2.4) an additional equation is necessary (assuming closed relationships are known for properties such as viscosity, conductivity and so forth). This is normally the perfect gas relationship, seen below:

$$P = \rho RT \quad (2.5)$$

where P is pressure, ρ is density, T is temperature, and R is the specific gas constant for the fluid involved. R can be related to the universal gas constant by the following formula:

$$R = \frac{R_u}{M} \quad (2.6)$$

where R_u is the universal gas constant, and \bar{M} is the molar mass of the gas in question. This gives a complete set of equations, relating density to local pressure and temperature at any location (12:40;15:258).

2.2 Turbulence Model

In the process of constructing a computational fluid dynamic model, a choice must be made about how to handle turbulence. If sufficient computer power were available, an incredibly fine mesh might be established, and no modeling would be necessary. This would require a mesh of hundreds of thousands or millions of elements for even the smallest problems, so this is impractical. One of the best accepted alternatives is a 2 equation model loosely based on the Bousinesq mixing length hypothesis (16;17;18:42). This hypothesis provides a model for turbulent viscosity, μ_t , where:

$$\mu_t = \rho l^2 \frac{\partial \bar{u}}{\partial y} \quad (2.7)$$

The problem is then to quantify the mixing length, l . Shih, Zhu, and Lumley provide a model in their paper (19) which uses 2 new partial differential equations for turbulent kinetic energy and turbulent dissipation to supplement the Navier-Stokes equations. In this case μ_t is defined through the following relation:

$$\mu_t = C_\mu \rho \frac{k^2}{\epsilon} \quad (2.8)$$

where k and ϵ are calculated from partial differential equations of the form:

$$\frac{Dk}{Dt} = \left[\left(\nu + \frac{\nu_t}{\sigma_k} \right) k \right] - \overline{u_i u_j} U_{i,j} - \epsilon \quad (2.9)$$

and

$$\frac{D\epsilon}{Dt} = \left[\left(\nu + \frac{\nu_t}{\sigma_\epsilon} \right) \epsilon \right] - C_{\epsilon 1} \frac{\epsilon}{k} \overline{u_i u_j} U_{i,j} - C_{\epsilon 2} \frac{\epsilon^2}{k} \quad (2.10)$$

where $C_{\epsilon 1}$, $C_{\epsilon 2}$, σ_k and σ_ϵ are all constants, specified in the model. This system allows the laminar stresses (due to the dynamic viscosity and the mean velocity gradients) and the turbulent stresses (modeled using μ_t and the mean velocity gradients) to be combined into a single stress, which can be calculated for each element in the flowfield. Using this system, the overall behavior of the flowfield can be modeled, including some of the turbulent effects, without excessive computational requirements. Since this did not exactly represent all of the possible loss mechanisms, it cannot capture all of the losses, but it should have captured the large majority of the losses and allowed more rapid determination of feasibility for the heat exchanger configurations under consideration (19).

2.3 Heat Transfer

2.3.1 Heat Flow in the Heat Exchanger. Since the heat exchanger was assumed to be manufactured from the hafnium isomer, the heat is generated within the solid isomer material of the heat exchanger. This is assumed to occur at a constant volumetric rate ($\frac{W}{m^3}$). Heat would then be convected off of the surface, or conducted along the surface. The heat flow in a control volume is shown in Figure 2.1. In steady state operation, the total of the heat fluxes on a control volume must be zero (i.e. $\dot{q}_{generated} + \dot{q}_{cond.in} - \dot{q}_{cond.out} - \dot{q}_{conv.} = 0$). Since the \dot{q} for conduction is given by:

$$\dot{q}_{cond.} = k \frac{dT}{dr} t \quad (2.11)$$

and $\dot{q}_{generated}$ is given by:

$$\dot{q}_{generated} = (HGR)dV \quad (2.12)$$

where k is thermal conductivity, t is thickness, $\frac{dT}{dr}$ is the temperature gradient, HGR is the volumetric heat generation rate, and dV is the volume of the differential control

volume, if the heat generation rate, geometry, and heat convection rate were known, the temperature gradient required could be calculated.

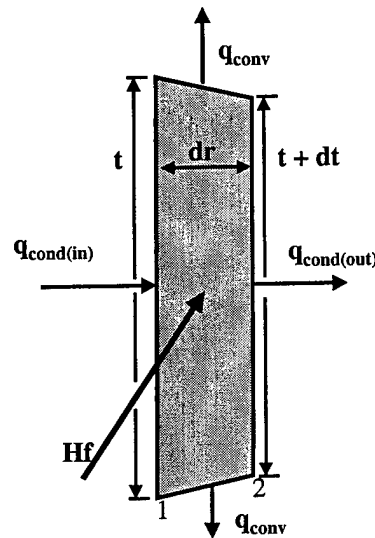


Figure 2.1 Differential Control Volume for Heat Flow Calculations

2.3.2 Convection. In general, heat transfer is a case of heat flowing from a high temperature material to a lower temperature material. In fluid mechanics the heat transfer rate per unit area (heat flux) \dot{q}'' is proportional to the difference in temperature between the fluid and the solid wall, as shown in Equation 2.13:

$$\dot{q}'' = h_f(T_{wall} - T_{\infty}) \quad (2.13)$$

The constant of proportionality, h_f , is the heat transfer coefficient. The challenge is to accurately determine h_f for the local conditions. The functions for determining h_f are part of the ANSYS®/FLOTRANTM program (11), but a check on the output for realism was desirable. For fully developed flow between two flat plates, Kays and Crawford (9:332) list the Nusselt number (based on hydraulic diameter), Nu_{D_h} ($Nu_{D_h} = \frac{h_f D_h}{k}$, where k is the conductivity of the fluid) as 378 for a Reynolds number

of 30,000 and Prandtl number of 0.7. For hydraulic diameter D_h ($D_h = \frac{4 \cdot \text{Area}}{\text{perimeter}} = 2 \cdot \text{spacing}$ for flat plates), of 9 mm and thermal conductivity, $k = 49.53$ milliwatts per meter Kelvin ($\frac{mW}{m \cdot K}$), this would make h_f about $2,000 \frac{W}{m^2 K}$ in fully developed flow between flat plates 4.5 mm apart. This is somewhat sensitive to temperature, as k is temperature dependent for air, but at temperatures likely to exist in a gas turbine, conductivity, k , is between 25 and $100 \frac{mW}{m \cdot K}$, so this estimate of h_f should not change overly much.

A further correlation for Nusselt number is presented in Hill and Peterson's book, *Mechanics and Thermodynamics of Propulsion*(20:129). Again, this is based on fully developed, turbulent flow, but in smooth tubes. In this correlation (Equation 2.14), the Nusselt number is proportional to the product of the $\frac{4}{5}$ power of Reynolds number and the cube root of the Prandtl number:

$$Nu_{D_h} = 0.023(Re_{D_h})^{0.8}(Pr)^{0.33} \quad (2.14)$$

Thus, for a given Reynolds number and Prandtl number, the Nusselt number is a constant. This does not, however, translate to constant heat transfer coefficients. As the temperature changes there will be small changes to the Reynolds number and Prandtl number, as well as the thermal conductivity of the air. The equation can be rearranged to give an explicit statement of h_f as:

$$h_f = 0.023(\rho c_p \bar{U}) \left(\frac{\bar{U} D_h}{\nu} \right)^{-0.2} \left(\frac{\mu c_p}{k} \right)^{-0.67} \quad (2.15)$$

This gives an additional estimate of the heat transfer coefficients expected. Using data for stagnation conditions entering the heat exchanger, and a typical velocity: $\bar{U} = 29$ m/s, μ is $3.1 \cdot 10^{-5} \frac{kg}{ms}$, ρ is $6.45 \frac{kg}{m^3}$, c_p is $1110 \frac{J}{kg \cdot K}$, k of $0.063 \frac{W}{m \cdot K}$ and D_h is 0.009 m. This yields a h_f of $688 \frac{W}{m^2 K}$ (20:129). This is significantly lower than the estimate from Kays and Crawford, but since these correlations are based

on slightly different flows (smooth tubes and flat plates), some difference would be expected. These two estimates did provide an idea of the order of magnitude the heat transfer coefficients should fall into.

In either case, most of the flow for the geometries used in this research will be thermal entry length flow. This should mean the h_f will be significantly higher (10-20% or more) at the leading edge of the heat exchanger fins, and asymptotically approach the fully developed flow condition as the fin length becomes very large. From Kays and Crawford (9:340) we can estimate the $\frac{x}{D_h}$ for the Nusselt number to reach the fully developed value at around 35. Since the heat exchangers used in this research have a fin length of 0.254 m and a D_h around 0.009 m, it is easy to show that the $\frac{x}{D_h}$ will not exceed about 28. Therefore, the flow will probably not be fully developed, and all of our Nu_{D_h} , and thus, all h_f s should exceed the fully developed flow conditions. There are a number of variables which affect the Nusselt number though. Increased surface roughness will tend to increase the Nusselt number, as will the square corners used on all heat exchanger fins in this research. The heat flux coefficient data from ANSYS® was not expected to match either of these correlations exactly, but it was expected to be of the same order of magnitude.

2.3.3 Pressure Losses Due to Heating. There is an inevitable loss of total pressure due to heating. This can be illustrated through the Rayleigh line flow, which describes the frictionless flow of compressible fluid in a constant area, heated duct. This can be derived from a one-dimensional momentum equation which reduces to:

$$p + \rho V^2 = \text{constant} \quad (2.16)$$

where p is pressure and ρ is density. Since the mass flux (mass flow/unit area), G , is constant, ρV^2 can be written as G^2/ρ , and Equation 2.16 can be rewritten as:

$$p + \frac{G^2}{\rho} = \text{constant} \quad (2.17)$$

Therefore, p reduces linearly with $1/\rho$, and since ρ decreases with increased temperature, p must also decrease with increased temperature. To keep mass flow constant, the speed must increase, which tends to offset some of the total, or stagnation, pressure loss, but this still results in an overall loss of stagnation pressure due to temperature increase (21:205-210;22:249).

More complex formulations will give the total pressure loss based on temperature change, inlet velocity, etc. These are shown below.

$$\frac{T_1(1 + \gamma M_1^2)^2}{M_1^2} = \frac{T_2(1 + \gamma M_2^2)^2}{M_2^2}$$

$$p_1(1 + \gamma M_1^2) = p_2(1 + \gamma M_2^2) \quad (2.18)$$

By solving these equations for given inlet conditions and a given outlet temperature, the outlet Mach number can be found. With the outlet Mach number, the outlet static pressure can be calculated, and the total pressure can be determined using isentropic relations. For the flows considered in this research, the temperature is rising from 622 K to approximately 1100 K, at inlet velocities around 40 m/s or a Mach number of 0.08. This combines to give a total pressure loss of about one percent, just due to temperature increase (21:205-210).

2.4 Gas Turbine Performance

2.4.1 On-Design Gas Turbine Performance. This section will concentrate mainly on the effects of turbine inlet temperature, T_{T4} , and burner pressure ratio, π_b , on the thrust of a turbojet engine. Using ONX, a software tool included with Mattingly, Heiser and Daley's *Aircraft Engine Design*(4;23), T_{T4} and π_b were varied to create Figure 2.2. As shown in Figure 2.2, increases in π_b and T_{T4} both lead to increased thrust, but there is obviously less limitation, and therefore more possible gain, to increases in T_{T4} .

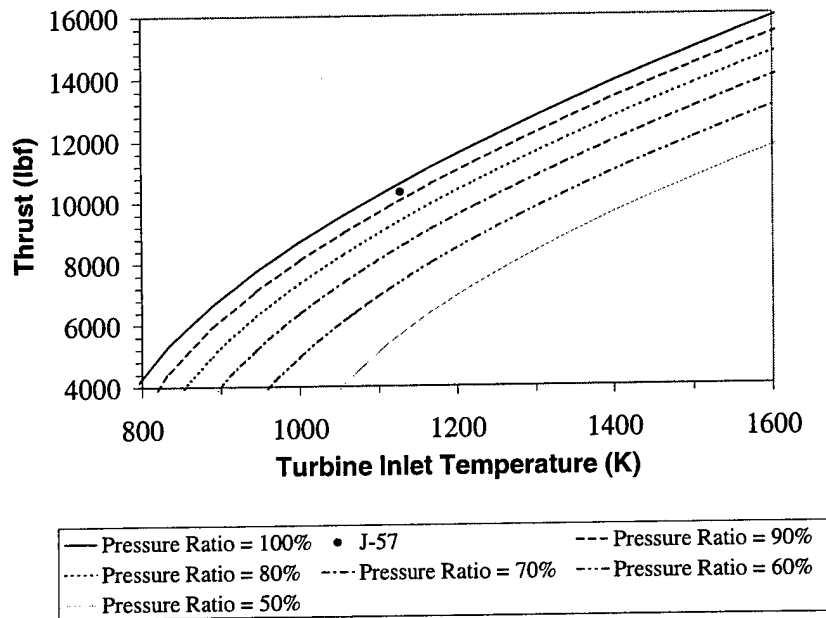


Figure 2.2 Burner Pressure Ratio and Turbine Inlet Temperature Effects on J-57 Thrust, from ONX

ONX estimates thrust by calculating pressure and temperature at each station through the engine, using the specified compressor pressure ratios, burner pressure ratios, turbine inlet temperature, and the efficiencies for diffusers, nozzles, compressors and turbines. The ONX program carries out all of the calculations based on inputs, calculates a work balance on the high and low pressure spools to determine the pressure and temperature ratios across the high and low pressure turbines, determines the fully expanded flow velocity at the outlet and an exit area per unit mass flow (23). These can be combined with a specified mass flow to calculate impulse at each station through Equation 2.19:

$$I_i = P_i A_i + \rho_i V_i^2 A_i \quad (2.19)$$

where I_i is the impulse, P is pressure, A is the area, ρ is density, and V is velocity, all at station i . We can rearrange these terms by recognizing that \dot{m} is ρAV , to get:

$$I_i = P_i A_i + \dot{m}_i V_i \quad (2.20)$$

The uninstalled engine thrust can be calculated by:

$$F = I_9 - I_0 - P_0(A_9 - A_0) \quad (2.21)$$

where F is the uninstalled thrust, subscripts denote the station number in the engine: station 0 is at the beginning of a streamtube leading to the engine inlet (for subsonic conditions) and station 9 is at the nozzle outlet, for a fully expanded nozzle. These terms can be further rearranged, assuming constant mass flow, or very small fuel flow relative to the air flow, to get:

$$F = \dot{m} \left[V_9 - V_0 + P_9 \frac{A_9}{\dot{m}} + P_0 \left(\frac{A_9}{\dot{m}} - \frac{A_0}{\dot{m}} \right) \right] \quad (2.22)$$

Therefore, since the mass flow through the engine is known, as are the pressures and temperatures, Mach number, velocity and area ratios can be calculated from isentropic compressible flow relationships (22:110-117). Since all of the quantities on the right hand side of Equation 2.22 are known or can be directly calculated, the uninstalled thrust can be easily calculated. This entire process was automated in ONX. In this case, a fully expanded nozzle was assumed, and, since this is uninstalled thrust, no inlet or boattail losses. This was deemed reasonable for the purposes of this research, since no airframe data was specified, and engine output is being compared to similar engines (4:225;23).

2.4.2 Off-Design Gas Turbine Performance. Off-design analysis of the operation of the J-57 was necessary to evaluate the effect of flight a higher altitudes on the heat exchanger. The program OFFX, also included with Mattingly, Heiser, and

Daley's book (4;23), was used to accomplish this. OFFX uses the engine specifications from ONX, including efficiencies for compressors, turbines, mechanical linkages, etc; along with the calculated high pressure turbine pressure ratio, which is constant when the low pressure turbine is choked, to calculate engine requirements away from the design point. By assuming that the low-pressure turbine is choked (which is true over a wide range of operating conditions), the high pressure turbine pressure ratio and corrected mass flow are held constant. OFFX requires inputs for the maximum allowable compressor pressure ratios, turbine inlet temperature, total temperature and pressure entering the burner, and high and low pressure spool speeds. OFFX can then perform a work balance on the high pressure spool to get the high pressure compressor pressure ratio, and maximize either compressor pressure ratio or turbine inlet temperature, without violating the other limitations, to calculate a thrust, mass flow, and other conditions through the engine, using methods similar to ONX. Using Data from OFFX, the burner entrance conditions at any flight altitude and Mach number could be found.

2.5 Triggered Hafnium Decay

The physics community has an interest in the 4 and 5 quasiparticle isomers of lutetium (Lu), hafnium (Hf), and tantalum (Ta), because they have relatively long half-lives, and high excitation energies. These long half-lives are possible because rapid decay is inhibited by the structure of the atomic nuclei. Since rapid decay to a lower energy state is inhibited, these isomers have a relatively long half-life. This is interesting because this represents a large amount of stored energy. In the isomer of interest to this research, $^{178}_{m2}\text{Hf}$, this stored energy is approximately 1.3 GJ/g, around one percent of the energy of a fission reaction (2;3).

Research shows that this energy can be released by bombarding the nucleus with X-rays at 10 to 90 keV. This has the effect of further raising the energy state of the nucleus, and freeing the nucleus from the structural prohibitions against rapid

decay. In this manner, the stored energy can be released at volumetric rates of up to $50 \text{ GJ/m}^3\text{s}$ (2)(3)(24). Since this reaction releases only photons, no particles, no change to the material properties of the hafnium was expected.

2.6 Radiation Shielding

The first step in determining the radiation shielding requirements would be to determine the radiation output from the source. In this case, to run the J-57 engine full throttle at sea level, the heat output to the air must be around 48 MW. This should represent about 95% of the total energy output of the hafnium, the remaining 5% being radiation (24). Therefore, the engine would have around 2.5 MW of radiation output. The equation for radiation dose is (25:369):

$$\dot{D} = \frac{CE \cdot 0.0027}{r^2 \cdot 4\pi} \quad (2.23)$$

where CE is the radiation generation rate in W and r is the radius from the source in m. If CE is 2.5 MW and r is about 3m, the dosage, \dot{D} is about 55 Grays/sec, or approximately 5,500 rem/s. A safe dosage for a human pilot, or similarly sensitive component, might be on the order of $1 \mu\text{rem/s}$ (25:369).

This leads to the shielding requirements for the pilot or other components. If it is assumed that all of the energy leaves the engine in the form of 600 keV gamma rays, deemed the most penetrating likely to escape the reaction process, and that lead shielding is used around sensitive areas, by consulting tables, one can find the mass attenuation ($\frac{\mu}{\rho}$) (Note that within this section only, μ is not viscosity, but an attenuation coefficient for radiation) to be about 0.13. Since the density of lead is about 11.4 g/cm^3 , this makes μ about 1.5 cm^{-1} . The thickness of shielding required to cut radiation by a given amount is calculated from (25:187):

$$x = \frac{-1}{\mu} \ln\left(\frac{n}{n_0}\right) \quad (2.24)$$

with μ in cm^{-1} , n the allowable dose behind the shielding, and n_o the potential dose without shielding, this gives the thickness, x , in cm. For this case, n is 10^{-6} rem/s, n_o is 5,500 rem/s, and μ is 1.5 cm^{-1} , making x about 15 cm, or a shield load of $1,700\text{ kg/m}^2$, or 350 lb/ft^2 of shield required. This should not be taken as an absolute or very accurate number. This is a very low order estimate, which mainly goes to show the need for a significant mass of radiation shielding. The estimate above could be off by a significant factor, depending on the exact spectrum of radiation to be attenuated, the geometry involved, the exact choice of materials, and the overall design of the shield. Therefore, all that can be said with accuracy at this point is that the weight of the radiation shielding will be significant (hundreds or thousands of pounds), and that it will be highly airframe dependent (25:187).

III. Computational Setup

This chapter contains a description of the computational hardware, software, and methods used in this research.

3.1 Hardware

All computations for this research were accomplished on a Dell® Dimension XPS T700R personal computer. This computer was equipped with a 700 MHz Pentium III® processor, 384 Mb of RAM, and a 19" monitor.

3.2 Software

This research used the commercial software package, ANSYS® 5.6.1 (11). This package includes the FLOTRAN® computational fluid dynamics program. ANSYS® comes equipped with its own grid generation and is capable of analyzing many types of flows, from simple adiabatic, incompressible, laminar flows, to turbulent, compressible flows with heat transfer. Multiple solver options, advection options, turbulence models and wall treatments are available. Boundary conditions on velocity, pressure, temperature, heat flux, and heat generation are available and were used in this research.

3.3 Software Inputs

This section contains information about the various software settings used in this research. For an example of the steps and inputs required to create a heat exchanger model like those used in this research, see Appendix B.

3.3.1 Solver Settings. For all runs the following settings were used. All runs were transient solutions (run to steady state), compressible, thermal, and turbulent. The turbulence model used in all cases was the $k - \epsilon$ from Shi, Zhu and

Lumley (19), with the default constants. The solver was set for 5,000 time-steps, with 20 global iterations per time step, and the ANSYS® (11) default time-step termination criteria. All fluid properties were set to calculate in SI units, and reference conditions were set to match the J-57 compressor outlet conditions (shown later in Table 4.1). Stability, relaxation, and results capping values were left at the default values. The various equations used the following solvers: X-velocity, Y-velocity, and temperature used the tri-diagonal matrix algorithm solver (TDMA); pressure used the preconditioned conjugate residual solver (PCRS); and turbulent kinetic energy and dissipation equations used the preconditioned generalized minimum residual method (PGMR) (26:7.39,40). The advection options selected were: for momentum, compressible pressure and energy equations, the monotone streamline upwind method; and for turbulent equations, the streamline upwind Petrov/Galerkin method (26:7.21-24). The various settings were selected for the stability they demonstrated in the software verification process.

3.3.2 Geometry. Three basic geometries of heat exchanger were explored in this research: Concentric annular tubes, radial trapezoidal fins, and a dual annulus of rectangular fins. These were selected as simple geometries which should be manufactureable. Simplicity of form may be critical, since all of the heated surfaces would be made of the hafnium isomer and its alloyed materials, and thus, the heat exchanger would generate heat within the solid material of the heat exchanger. Given the extraordinary strength of hafnium (yield strength about 50% higher than titanium, ultimate strength over 100% higher (27:665)) machining may be quite difficult, so it would probably be helpful to keep manufacturing steps to a minimum. In addition, the flow through all of these geometries can be reasonably approximated by a series of two-dimensional flow fields. This was important, as a single three-dimensional run could have taken several weeks on a PC, or consumed a considerable amount of (very expensive) time on a faster computer system.

3.3.3 Concentric Tubes. With the concentric tubes, the flow is through an annulus made up of a number of concentric tubes, surrounding the drive spools of the engine. A schematic view of the cross section at section A-A of Figure 1.2 is shown in Figure 3.1. The flow between any two of the concentric tubes can be approximated as the flow between two flat plates, provided the ratio of the radii of the cylinders, $\frac{r_i}{r_o}$, is close to unity. Since the spacing used is small, and there is a relatively large minimum inner radius for the heat exchanger, this value, at a minimum is about 0.96 (9:327). Therefore, one can consider this a two dimensional flow with a streamwise, or axial direction and a radial direction. For this flow, two heat exchanger envelopes were used. The first, used for many runs to reduce computation time, used a 25.4 mm high inlet, expanding in 76.2 mm to a 50.8 mm high straight duct, 255 mm long, narrowing back to a 25.4 mm outlet, and attached to a long outlet duct (see Figures 3.2, 3.3 and 3.4). The small size of the geometry allowed a smaller number of elements, and a vastly reduced computation time to evaluate trends. This geometry did not correlate to anything which could be installed in a J-57 engine, and this was intentional. It was used solely as a tool for evaluating some trends and ideas in a timely manner. In this geometry, shown in Figures 3.2, 3.3 and 3.4 as the view of Section A-A of Figure 3.1, tubes from 0.5 mm thick to 2.0 mm thick were checked with about 4.5 mm spacing between them. With 0.5 mm tubes, both full length tubes, 254 mm long, and staggered tubes, 10 rows of 25.4 mm tubes offset 2.5 mm from each other were used.

The second geometry was generated to more closely match the actual size of the J-57 combustion chamber, and Figure 3.5 shows the view from Section A-A of Figure 3.1 for this geometry. This layout uses a 50.8 mm high inlet, expanding in 254 mm to a 206 mm high straight duct, 254 mm long, which contracts in 254 mm to a 76.2 mm high outlet, connected to a long outlet duct. This used 2.0 mm thick tubes, spaced 4.5 mm apart for the length to the 206 mm high duct section, to verify

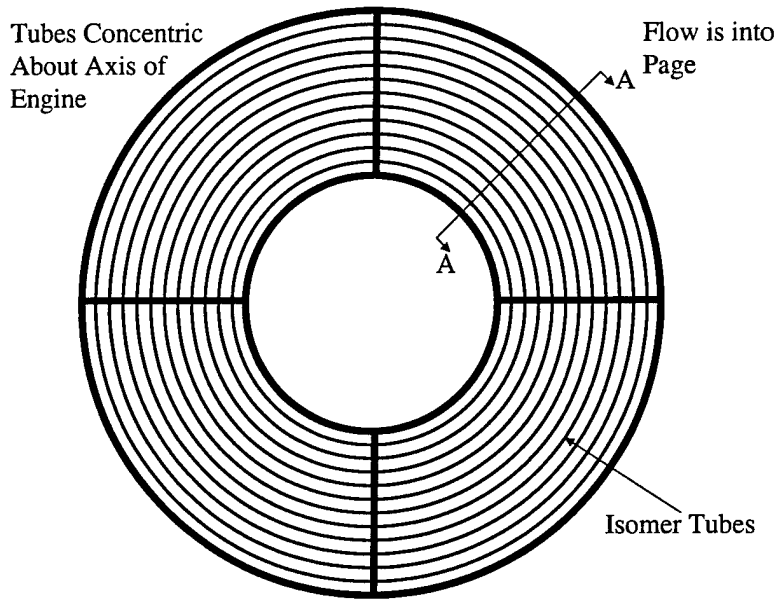


Figure 3.1 Schematic View of Concentric Tube Geometry

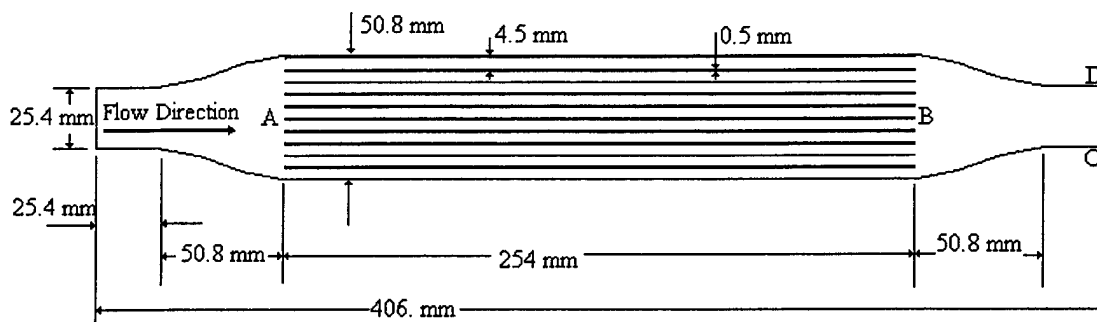


Figure 3.2 Model Geometry, 0.5 mm Thick Tubes, Compact Concentric Geometry (Cross-Section A-A of Figure 3.1)

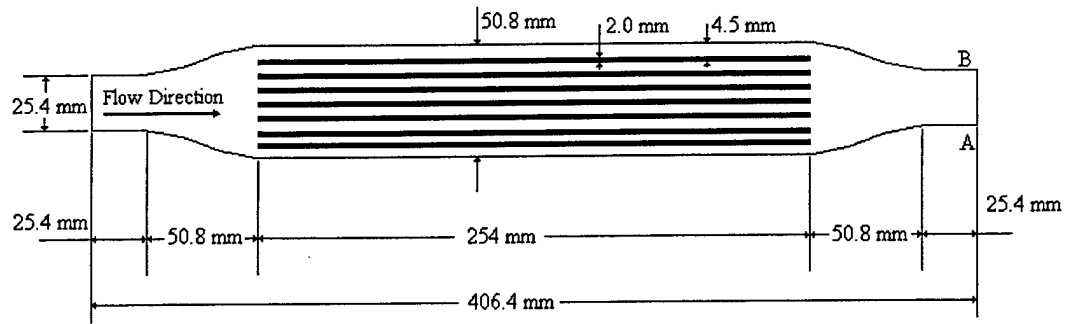


Figure 3.3 Model Geometry, 2.0 mm Thick Tubes, Compact Concentric Geometry (Cross-Section A-A of Figure 3.1)

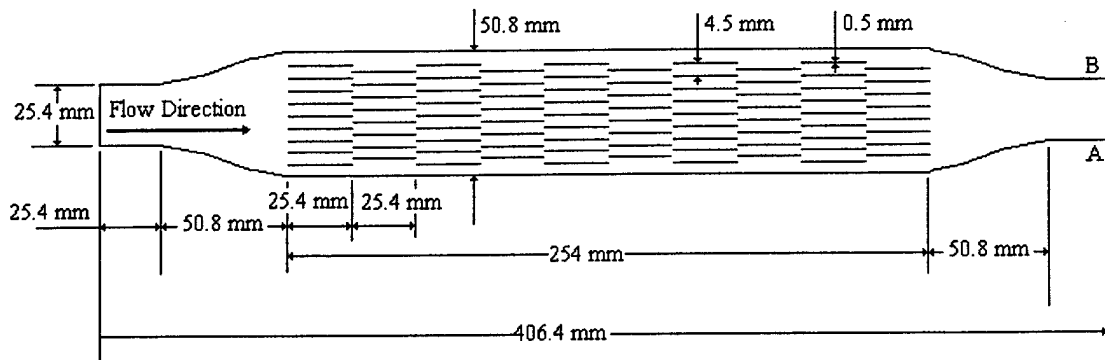


Figure 3.4 Model Geometry, 0.5 mm Thick Staggered Tubes, Compact Concentric Geometry (Cross-Section A-A of Figure 3.1)

the applicability of results from the smaller geometry, and evaluate altitude effects on the heat exchanger.

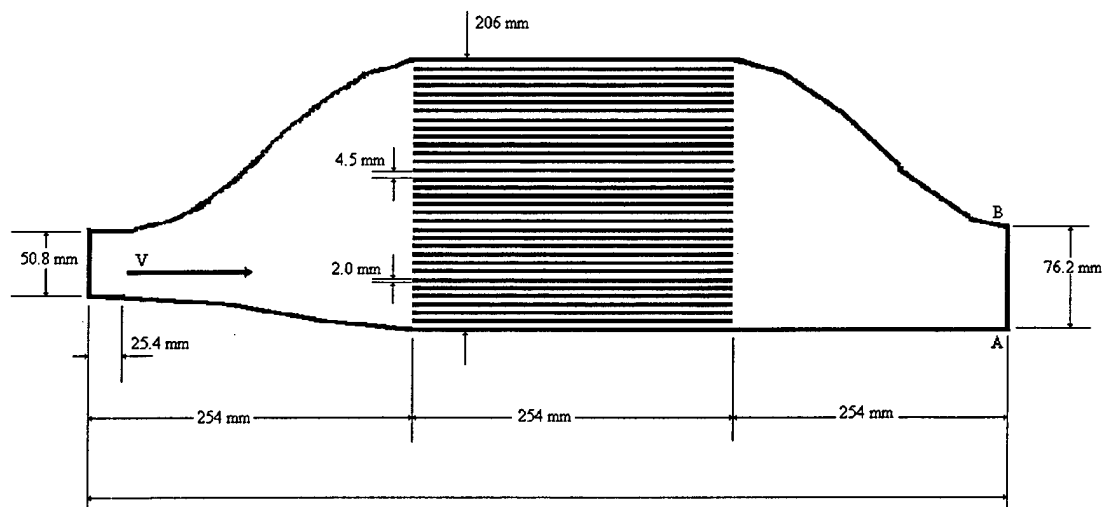


Figure 3.5 Model Geometry, 2.0 mm Thick Tubes, Full-Scale Concentric Geometry (Cross-Section A-A of Figure 3.1)

3.3.4 Trapezoidal Fins. The use of straight fins, for easier manufacturing, presented two options: either the thickness of the fins, or the space between the fins, must change with radius. For the trapezoidal fins, the thickness of the fins is changed with the spacing held constant. This is shown schematically in Figure 3.6 as the view from Section A-A of Figure 1.2, and an expanded view in Figure 3.7. This was treated as several cases of flow between flat plates, at the locations indicated in Figure 3.7 (sections A-A, B-B, and C-C). The geometry of a flat plate case is shown in Figure 3.8 and all radial fin geometries are similar. The dimensions of the geometry for each section are found in Table 3.1 (see Figure 3.8 for locations).

3.3.5 Rectangular Fins. With the rectangular fins, two annuli of straight, constant thickness fins were used. The view of Section A-A of Figure 1.2 is shown in Figure 3.9, and a close view of a pair of rectangular fins is shown in Figure 3.10. Two annuli were used to minimize the variation in spacing between the fins. For

Table 3.1 Dimensions of Geometries Used in Trapezoidal Fin Computations (see Figure 3.8 for Locations of Dimensions)

Location	Inlet H	Inlet L	Fin Spacing	Fin L	Outlet H	Outlet H
Inner Rad.	5.0 mm	25.4 mm	4.5 mm	254 mm	5.0 mm	220.6 mm
Mid. Rad.	6.5 mm	25.4 mm	4.5 mm	254 mm	6.5 mm	220.6 mm
Outer Rad.	8.3 mm	25.4 mm	4.5 mm	254 mm	8.3 mm	220.6 mm

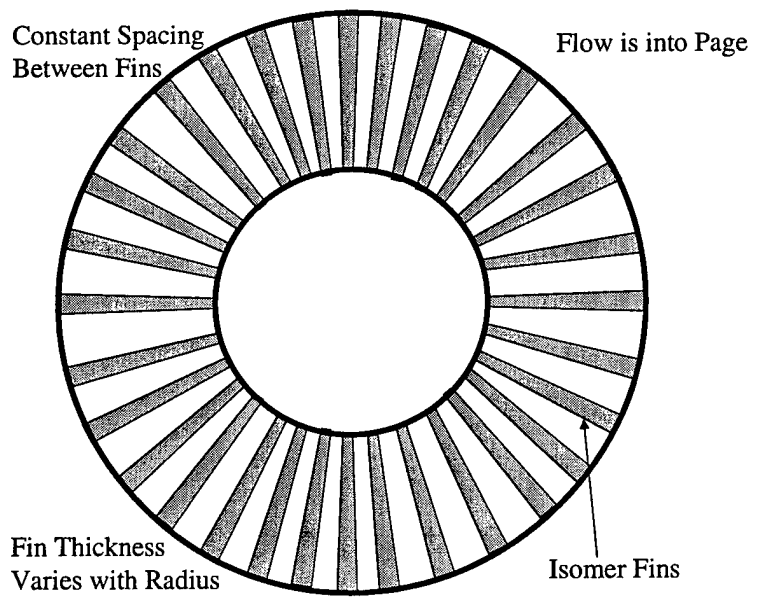
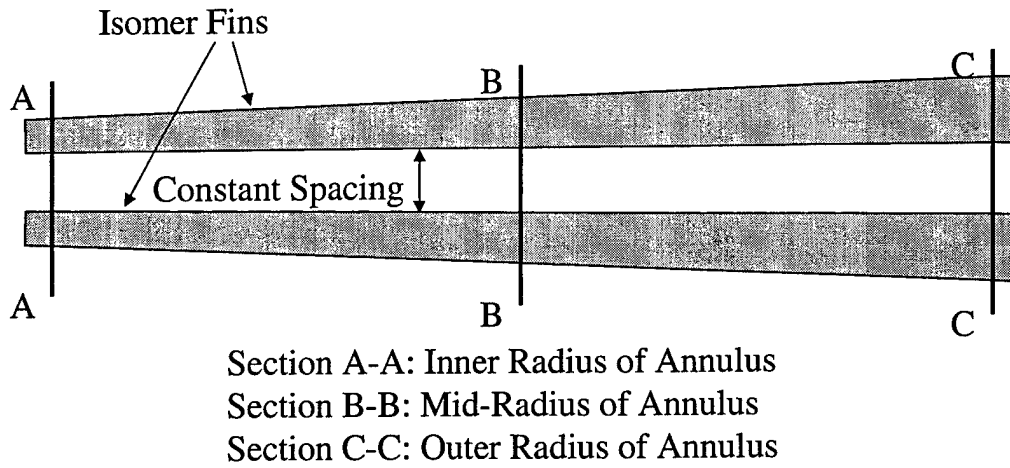


Figure 3.6 Schematic View of Trapezoidal Radial Fin Geometry



Flow is into Page

Figure 3.7 Schematic View of Two Trapezoidal Fins

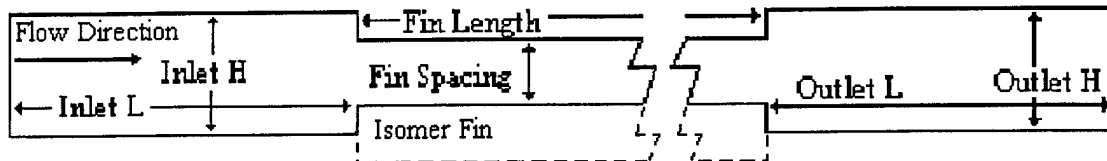


Figure 3.8 Example of Radial Fin Computational Geometry

each annulus, runs were done at the inner radius (section A-A of Figure 3.10), outer radius (section B-B of Figure 3.10), and center (section C-C of Figure 3.10) of each annulus, to establish a variation across the annulus. Construction of each model was similar to the trapezoidal models (see Figure 3.8), except that ledges were all 1.0 mm high, for a 2.0 mm thick fin, and spacing was varied. Dimensions are found in Table 3.2, for each of the rectangular fin computational models.

Table 3.2 Dimensions of Geometries Used in Rectangular Fin Computations (see Figure 3.8 for Locations of Dimensions)

Location	Inlet H	Inlet L	Fin Spacing	Fin L	Outlet H	Outlet H
Inner Annulus						
Inner Rad.	5.55 mm	25.4 mm	3.55 mm	254 mm	5.55 mm	220.6 mm
Mid. Rad.	6.5 mm	25.4 mm	4.5 mm	254 mm	6.5 mm	220.6 mm
Outer Rad.	7.45 mm	25.4 mm	5.45 mm	254 mm	7.45 mm	220.6 mm
Outer Annulus						
Inner Rad.	5.77 mm	25.4 mm	3.77 mm	254 mm	5.77 mm	220.6 mm
Mid. Rad.	6.5 mm	25.4 mm	4.5 mm	254 mm	6.5 mm	220.6 mm
Outer Rad.	7.22 mm	25.4 mm	5.22 mm	254 mm	7.22 mm	220.6 mm

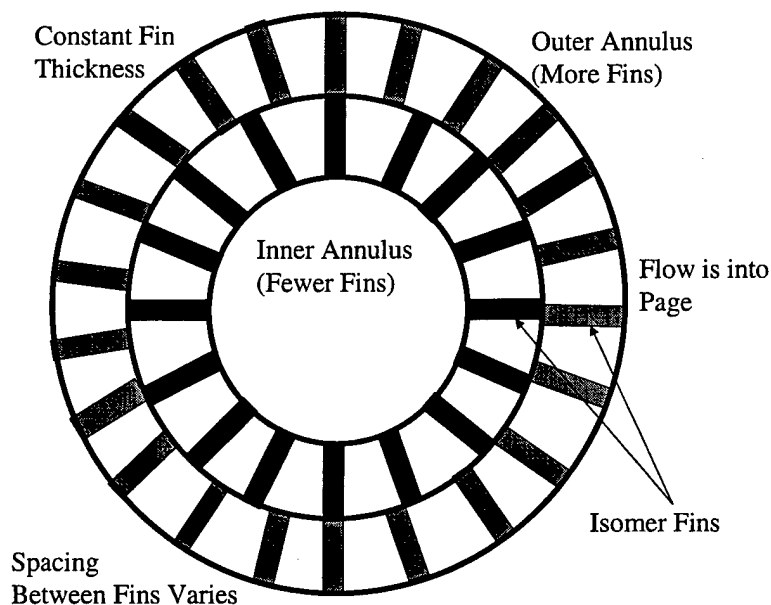
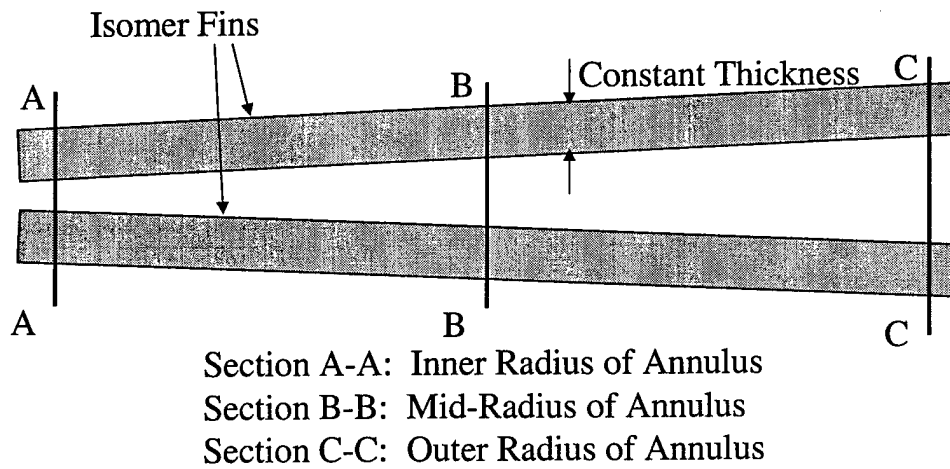


Figure 3.9 Schematic View of Rectangular Radial Fin Geometry



Flow is into Page

Figure 3.10 Schematic View of Two Rectangular Fins

3.3.6 Radial Fin Inlet and Outlet. These two sections were done to provide estimates of the pressure losses heading into and out of the radial fin geometries. The inlet and outlet were created to match the J-57 geometry. The inlet was 254 mm long, expanding the flow from a 50.89 mm inlet height to a 206 mm outlet height (see Figure 3.11). The outlet section was 254 mm long, compressing the flow from the 206 mm height to a 76.2 mm outlet (see Figure 3.12). Each of these had a 746 mm straight duct attached to the outlet to allow the outlet pressure boundary condition to be separated from the area of interest. Flow data was taken at the inlet and across the exit of the 254 mm long area of interest.

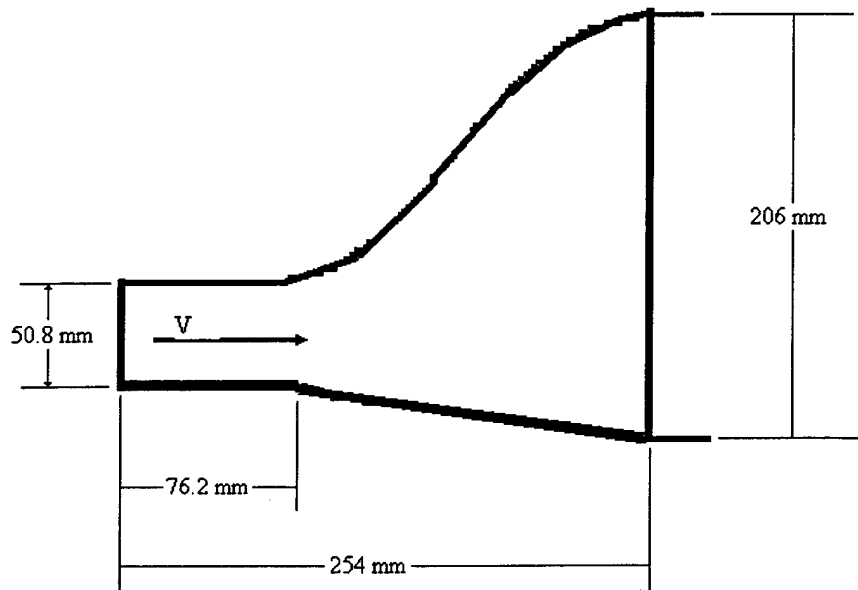


Figure 3.11 Radial Geometry Inlet

3.3.7 Grid Generation. All computational domains were created using the built-in tools of ANSYS®/FLOTRANTM (11). The meshes were constructed using unstructured triangular elements. These were selected due to the irregular geometries of many domains, and a restriction in the software against meshing some irregular shapes with quadrilaterals. There are potential drawbacks to this type of

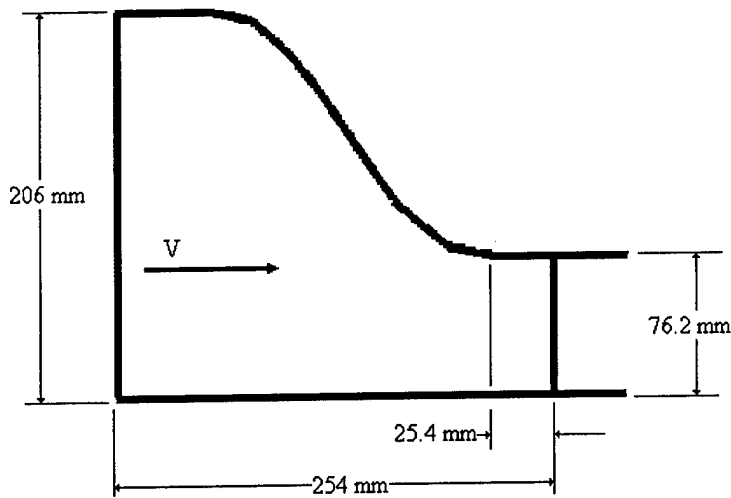


Figure 3.12 Radial Geometry Outlet

mesh, but to minimize these, element sizes were kept small in the areas of interest to keep y^+ ($y^+ = \frac{y(\frac{\tau_w}{\rho})^{0.5}}{\nu}$) values in the 10 - 5,000 range recommended by ANSYS® (28). Outside the areas of interest, in the exit ducts from the heat exchanger sections, elements were made as large as possible to decrease computational time. Since these ducts were only present to move boundary conditions well away from the points where data was taken, this was judged to have few drawbacks.

3.3.8 Reference Conditions. All reference conditions were calculated from the compressor output conditions for the J-57 engine, using OFFX for operating conditions other than static, sea level. Reference pressure was 1.15 MPa for static sea level runs (167 psia), reference temperature was 622 K (1120 °R) (29:474). All fluid properties (viscosity, density, conductivity) were calculated based on the computed static pressure and temperature at each location. However, ANSYS® (11) did not allow variable specific heats with a compressible flow. Therefore, a specific heat of 1004 J/kgK was used, and the data was corrected at the end to account for the

specific heat variation. The correction process can be found in Appendix A. Using OFFX, combustion chamber entrance conditions were calculated at Mach 0.8 for altitudes of 15,000 ft, 30,000 ft and 45,000 ft.

3.3.9 Boundary Conditions. For all runs, similar boundary conditions were applied. First, all solid boundaries were represented by conditions of zero velocity in both the x and y directions. Inlet velocity was entirely in the x direction. The compact concentric geometries were run with inlet velocities of 75 m/s, and in the full scale concentric fin case, the inlet velocity was determined from the J-57 mass flow and the inlet annulus area (112 m/s at sea level, 104 m/s at 15,000 ft, 99 m/s at 30,000 ft, and 95 m/s at 45,000 ft). For the radial fin geometries, the inlet velocities were run at two levels: the first, at 41 m/s was to closely match the compact concentric geometry results for comparison; the second, at 29 m/s was to match the one-dimensional expansion from the J-57 burner inlet to the nominal heat exchange height (a 1:4 ratio). The second velocity should closely match the actual velocities in the J-57 burner which should 25-30 m/s at sea level static operation. At the outlet from the models, pressure was set to zero, relative to the pressure offset input.

3.3.10 Thermal Boundary Conditions. To establish the proper heat transfer boundary condition for the flow, three possible cases were evaluated: constant wall temperature, constant heat flux (at the fin or tube surface), and constant volumetric heat generation (within the fin or tube material). Since the hafnium isomer was assumed to make up the entirety of the heat exchanger fins or tubes, the heat would be generated within the body of the fins or tube themselves. The fins or tubes were assumed to be manufactured from hafnium because hafnium is a structurally strong metal (the yield strength of hafnium is 50% greater than that of titanium) (27:665), and the surface temperatures involved would melt most other materials. The constant heat generation was assumed to be the most accurate model of the

isomer decay process, and the best heat transfer boundary condition. However, it is also the most computationally intensive, as it requires the temperature to stabilize in the material, which takes a significant amount of time (An early estimate with small models indicated that the run time for a constant heat generation case would be approximately one month). Therefore, it was decided to select one of the other boundary conditions, which do not require convergence to their own steady state before the flow can begin to converge. To decide between constant wall temperature or constant heat flux, it was decided to go with the condition whose temperature gradient most nearly matched the constant heat generation condition. The variation of temperature distributions is shown in Figure 3.13.

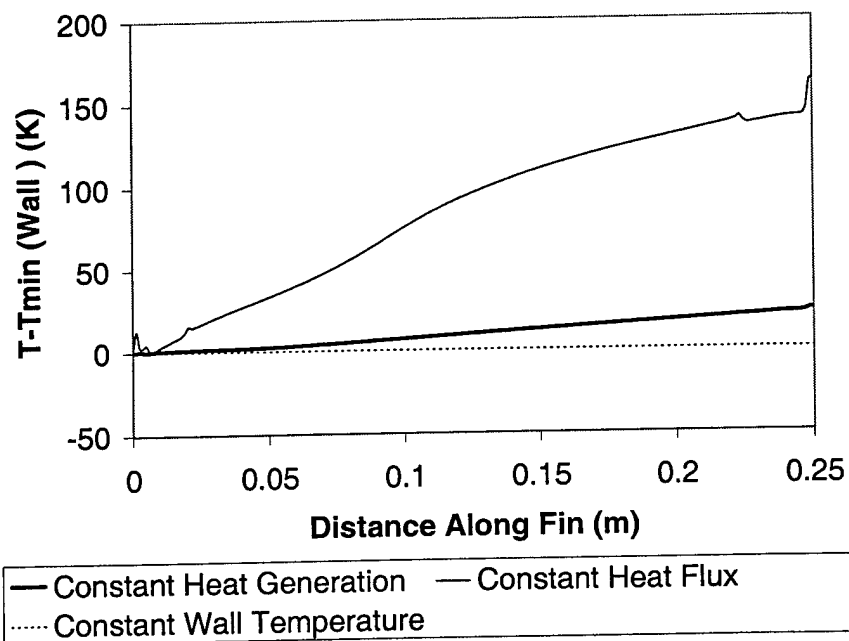


Figure 3.13 Variation of Wall Temperature along Fin/Tube Surface

The constant wall temperature, of course has no variation in temperature along the plate. The constant heat flux shows a variation of about 660 K/m, and the constant heat generation shows a variation of about 120 K/m. The mechanism for the difference between constant heat flux and constant wall temperature was the conduction through the material of the fin. The trailing edge of the fin generates

heat which cannot be removed by convection, since the heat transfer coefficients are lower, so this heat was conducted toward the leading edge, where the heat transfer coefficients are higher, and the heat can be convected away. For all computations in this research, a constant wall temperature of 2400 K was applied to the surfaces of the hafnium isomer fins or tubes, and all other solid surfaces were considered insulated (zero heat flux boundary condition applied). This temperature (2400 K) was chosen as a reasonable margin below the melting point of hafnium (around 2500 K) (27:665).

It is worth noting that, where there are significant changes in fin thickness, this may be a very poor assumption. If an energy balance is performed on a small control volume of fin, as shown in Figure 2.1, it can be shown that, if the net increase in stored energy within the control volume is zero (steady state operation):

$$q_{generated} + q_{cond.in} - q_{cond.out} - q_{conv.} = 0 \quad (3.1)$$

where these quantities are given by:

$$\begin{aligned} q_{generated} &= (HGR) \cdot \frac{2t + dt}{2} dr \\ q_{cond.in} &= k \left. \frac{dT}{dr} \right|_1 t \\ q_{cond.out} &= k \left. \frac{dT}{dr} \right|_2 (t + dt) \\ q_{conv.} &= 2h_f(T_w - T_\infty) dr \end{aligned}$$

and HGR is the volumetric heat generation rate. If HGR is taken to be $1 \cdot 10^9 \frac{W}{m^3}$ (the approximate level required for J-57 operation at sea level with the trapezoidal fin geometry), $k = 22 \frac{W}{mK}$, and $h_f = 700 \frac{W}{m^2K}$ (a reasonable average value for the observed data) it can be quickly shown that very large magnitudes of $\frac{dT}{dr}$ are required at both extremes of the trapezoidal fins to balance the energy in the control volume. At the thick end ($t = 3.8 \text{ mm}$), $\frac{dT}{dr}$ must be large to conduct heat away from the

control volume, while at the thin end ($t = 0.5$ mm), $\frac{dT}{dr}$ must be very large to conduct heat into the control volume. In either case, to assume constant volumetric heat generation and constant wall temperatures in the radial direction, the fins must be nearly constant thickness, or they must be hollow, or filled with neutral material, such that the volume distribution of isomer is nearly constant at any radius along the fin. If solid fins, varying in thickness from 0.5 mm to 3.8 mm were used, the temperatures could vary hundreds to thousands of degrees from the inner radius to the outer radius. In the constant thickness fins, there must be some temperature gradient ($\frac{dT}{dr}$) to account for heat transfer from the inner radius (where h_f would be low) to the outer radius (where h_f would be higher), but these would be much smaller (on the order of 100 K across the radial span of each fin (103 mm), and therefore a maximum temperature difference on the order of 50 K at any point), and negligible in light of the normal accuracy of heat transfer calculations.

Therefore, while constant temperature in both the axial and radial directions is a reasonable assumption for constant (or nearly constant) thickness fins or tubes, if the thickness changes significantly (as in the constant spacing radial fin geometry), this may be very misleading. The exception to this would be a tapered fin which is manufactured hollow (forming a V in cross section), so that the total thickness of material is nearly constant in the radial direction. In this research, to assume solid trapezoidal fins (of the dimensions specified) would probably require fin temperatures in excess of the melting point of hafnium to maintain the overall levels of heat transfer obtained here. The data presented in this research for that geometry would only be possible with fins made up of two thin plates forming the trapezoidal fin (possibly filled with some material which would not contribute to the heat generation, but which would contribute structural support).

3.4 Code Validation

In preparation for conducting this research, ANSYS®/FLOTTRAN® (11) was used to replicate the results of research conducted by Jarcy (30) in evaluating the flow field behind a heated cylinder in crossflow. Using identical geometry and test conditions, a very similar total pressure profile was obtained behind the cylinder. The profile obtained was judged even better when the effects of the relatively large pitot probe used by Jarcy to obtain his data were considered. With the inevitable smearing of sharp pressure gradients induced by the pitot probe, the experimental data and computational data are very close. All of the settings feeding into the turbulence model were maintained throughout the research (30;31).

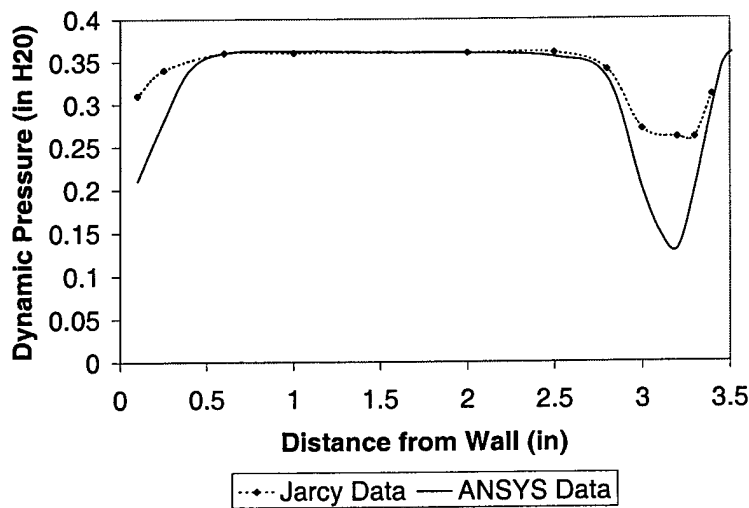


Figure 3.14 Comparison of Experimental and Computational Dynamic Pressure Distributions Behind a Cylinder in Crossflow

Table 3.3 Comparison of Temperature Distributions on a Cylinder in Crossflow

Location in Degrees from Stagnation Point	Experimental Temperature ($^{\circ}F$)	Computational Temperature ($^{\circ}F$)
0	553	561
90	734	651
180	739	728

IV. Results and Discussion

This chapter contains the results of the computational models in the present work. The estimated performance of the various heat exchanger geometries in a J-57 turbojet is also provided.

4.1 Pressure Ratios and Total Temperature Increases

All data is provided in terms of average total pressure ratio (expressed in a percentage, outlet over inlet) and an average total temperature. For the reduced size geometries for concentric tubes, these are algebraic averages, while for all others, an area-weighted average is used ($\frac{1}{A} \sum quantity \cdot \delta A$). This should provide the best estimate of the turbine inlet conditions for the operating gas turbine engine. Note that all temperatures in charts are uncorrected, but corrected temperatures have been used in all performance estimates. Overall results (corrected temperatures and pressure ratios) can be found in Table 4.6.

4.1.1 Concentric Tube Geometry. The first section run used the compact geometry for 0.5 mm thick concentric tubes. Again, this geometry was not intended to correlate to anything installed in the J-57 turbojet, it was solely intended to examine trends and options in a timely manner (the reduced size led to reduced computation time). The outlet conditions for this are shown in Figure 4.1, as they vary from the inner (lower) wall of the geometry shown in Figure 3.2 (location C) to the upper wall (location D). As one would expect, the total pressure is nearly constant across the outlet, while the total temperature has not yet mixed enough to reach a near uniform condition. The (algebraic) average outlet conditions for this geometry are: $T_{T4} = 1090$ K (1962°R), and $\pi_b = 96.76\%$. This T_{T4} corrects to 1027 K (1848°R) (see Table 4.6 for comparison to other geometries).

An item of interest was to evaluate the heat transfer coefficients for reasonableness. Figure 4.2 is a plot of the computed heat flux and heat transfer coefficient variation along the center (fifth from the bottom) tube/fin of the geometry shown in Figure 3.2, starting at the left (location A) and going along the upper surface of the tube/fin to location B. As shown in Figure 4.2, the heat transfer coefficient has a high of about $1,000 \text{ W/m}^2\text{K}$ and a low of about $700 \text{ W/m}^2\text{K}$. This is well short of the value of about $2,000 \text{ W/m}^2\text{K}$ for fully developed turbulent flow between two flat plates predicted by Kays and Crawford (9:326). However, it is very close to the value of $688 \text{ W/m}^2\text{K}$ calculated from Hill and Peterson (See Section 2.3.2 of this document)(20:129). The leading edge h_f is about 30% higher than the trailing edge, and the data shows overall excellent agreement with the expected results. Therefore, the ANSYS® (11) data was taken as a reasonable approximation of reality. Other concentric tube geometries showed behavior similar to Figure 4.2.

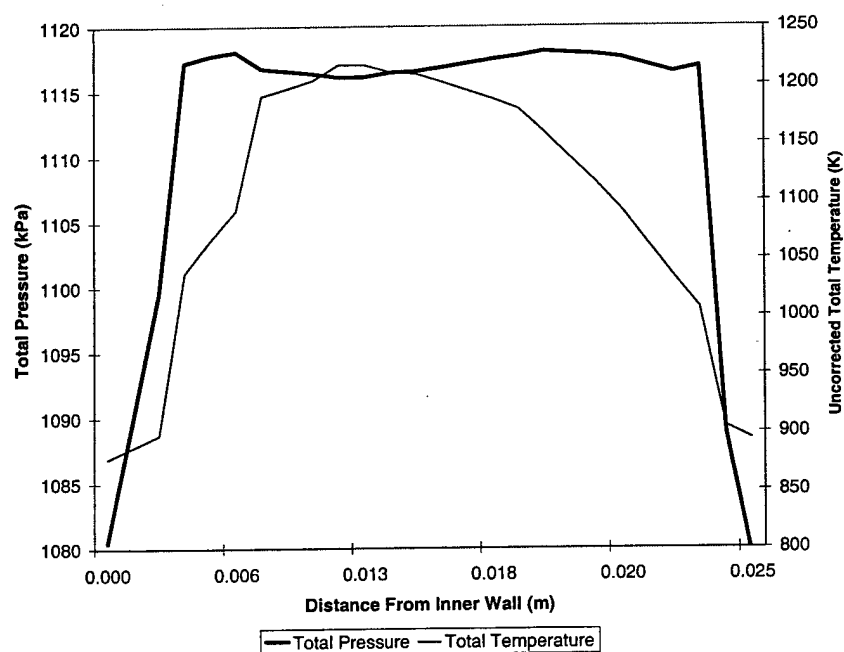


Figure 4.1 Radial Variation of Total Temperature and Total Pressure Across Exit Plane (Location C to Location D in Figure 3.2), Compact Concentric Tube Heat Exchanger, 0.5 mm Thick Tubes

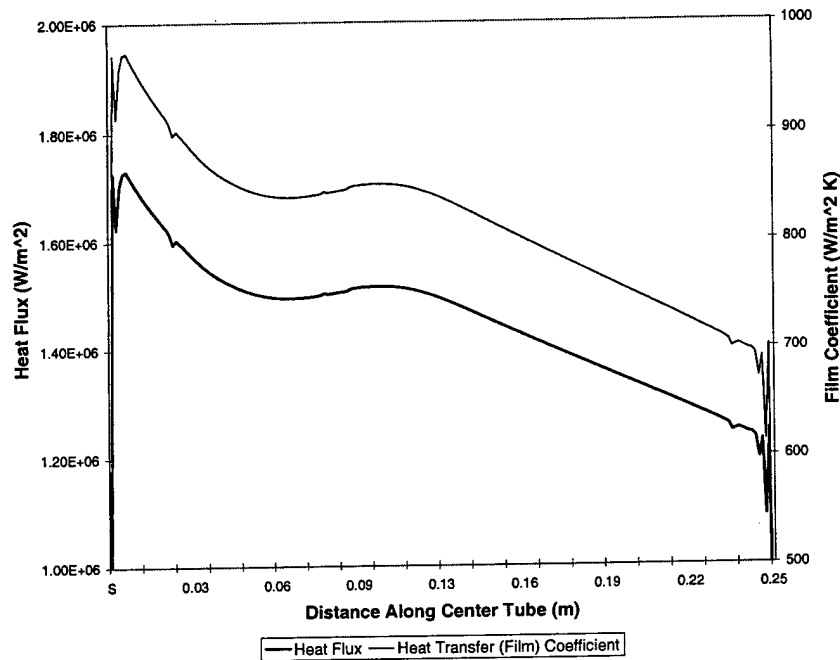


Figure 4.2 Axial Variation of Heat Flux and Heat Transfer Coefficient on Center Tube (Location A to Location B in Figure 3.2), Compact Concentric Tube Heat Exchanger, 0.5 mm Thick Tubes

Two additional configurations were run with the compact concentric tube geometry (see Figures 3.1, 3.2, and 3.3 for illustrations). The first used fins 2.0 mm thick instead of 0.5 mm thick (see Figure 3.3). This was done to evaluate the pressure and temperature effects of thicker tubes, as might thicker tubes might be required for structural integrity or ease of manufacture. With the total heat exchanger height the same, and maintaining constant spacing between the tubes, this resulted in fewer tubes. Results are shown in Figure 4.3, as the total temperature and total pressure distributions across the exit of the heat exchanger from the lower/inner wall (location A in Figure 3.3) to the upper wall (location B). The average conditions were: $T_{T4} = 1042 \text{ K}$ (1876°R), and $\pi_b = 97.01\%$. This corrects to 986 K or 1774°R (see Table 4.6 for comparison with other geometries). The T_{T4} seems low, but some of this is due to the space between the inner wall and the first tube being somewhat larger. If the outer half of the data points were used, the average T_{T4} would be 1092

K (1966°R)(which corrected to 1028 K or 1851°R). The somewhat lower pressure losses can be attributed to the lower temperature rise, combined with lower viscous losses due to less exposed surface area.

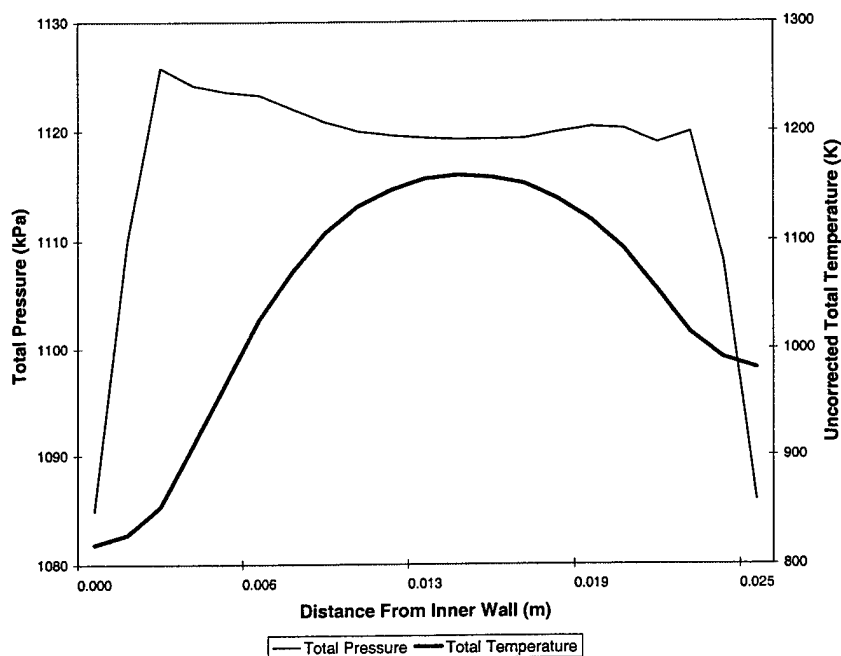


Figure 4.3 Radial Variation of Total Temperature and Total Pressure Across Exit Plane (Location A to Location B, in Figure 3.3), Compact Concentric Tube Heat Exchanger, 2.0 mm Thick Tubes

The last configuration run with the compact concentric tubes uses staggered rows of tubes, each 25.4 mm long, offset by 2.5 mm (this geometry is shown in Figure 3.4). This was done to evaluate the possibility of significantly increased heat transfer. Higher heat transfer was expected because almost the entire surface area of the heat exchanger would be in the very beginning of the thermal entry length, since each row of tubes would start a new entry length. Therefore, the heat exchanger would have the highest possible heat transfer coefficients throughout. Results are shown in Figure 4.4 (total temperature and total pressure distributions from location A in Figure 3.4 to location B), and the average outlet conditions are: $T_{T4} = 1108$ K (1994°R) and $\pi_b = 95.0\%$. The corrected T_{T4} is 1042 K, or 1875°R. There is a small

improvement in heat transfer, but the relatively large increase in pressure loss and increased complexity would likely offset the small possible performance gains (refer to Table 4.6 for performance comparisons).

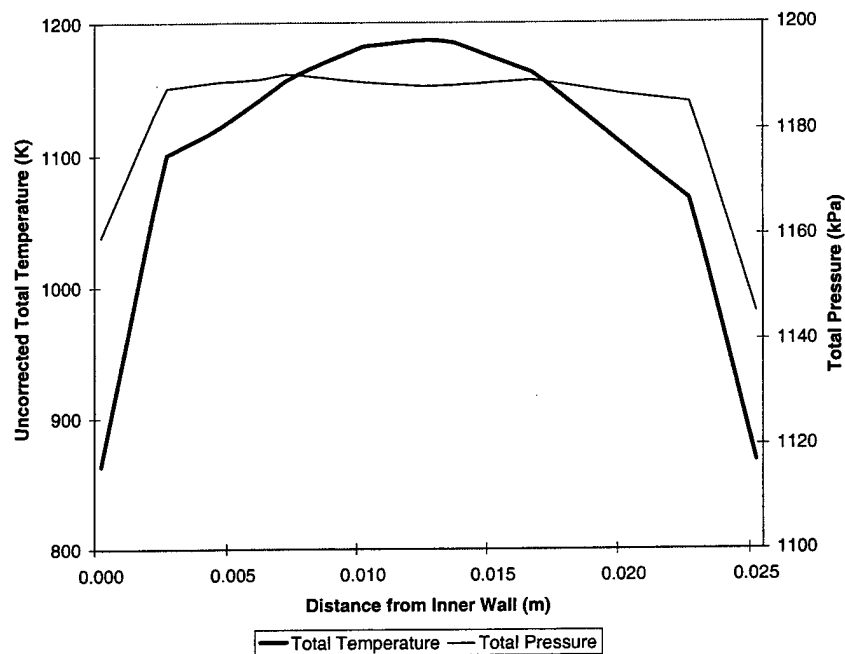


Figure 4.4 Radial Variation of Total Temperature and Total Pressure Across Exit Plane (Location A to Location B in Figure 3.4), Compact Concentric Tube Heat Exchanger, 0.5 mm Thick Staggered Tubes

A final geometry was evaluated with the concentric tubes. This was a full scale model, which would simulate an annular heat exchanger fully replacing the burner section of a J-57 (see Figures 3.1 and 3.5. The overall length is 76.2 cm (30 inches), and the heat exchanger has a maximum height of 20.6 cm (8 inches). The tubes are 2 mm thick, 4.5 mm apart, and 25.4 cm long (10 inches). Higher total temperatures were expected out of this geometry for two reasons: First, the cooling passages at the upper and lower wall make up far less of the total flow; Second, the flow entering the fins should be a lower velocity than evaluated in the compact geometry. Even though the lower velocity would indicate a lower Reynolds number, and therefore lower heat transfer coefficients, we would expect the outlet temperature to increase,

since the mass flow through any given channel decreases faster than the heat transfer coefficient ($h_f \propto Re_{D_h}^{0.8}$ while $\dot{m} \propto Re_{D_h}$). Since the total heat added to the flow does not decrease as fast as the mass flow, the temperatures must increase. Higher pressure losses were also expected, due to larger temperature increases, and higher diffusion/compression ratios for the inlet and outlet manifolds, although this would be balanced somewhat by the lower viscous losses due to the lower velocities on the tubes. Overall distributions for outlet total temperature and pressure are shown in Figure 4.5, from the inner radius (location A in Figure 3.5) to the outer radius (location B in Figure 3.5). The average (area weighted) T_{T4} was 1236 K (2224°R) and π_b was 94.5%. This led to a corrected T_{T4} of 1150 K (2070°R) (see Table 4.6 for performance comparisons to other geometries).

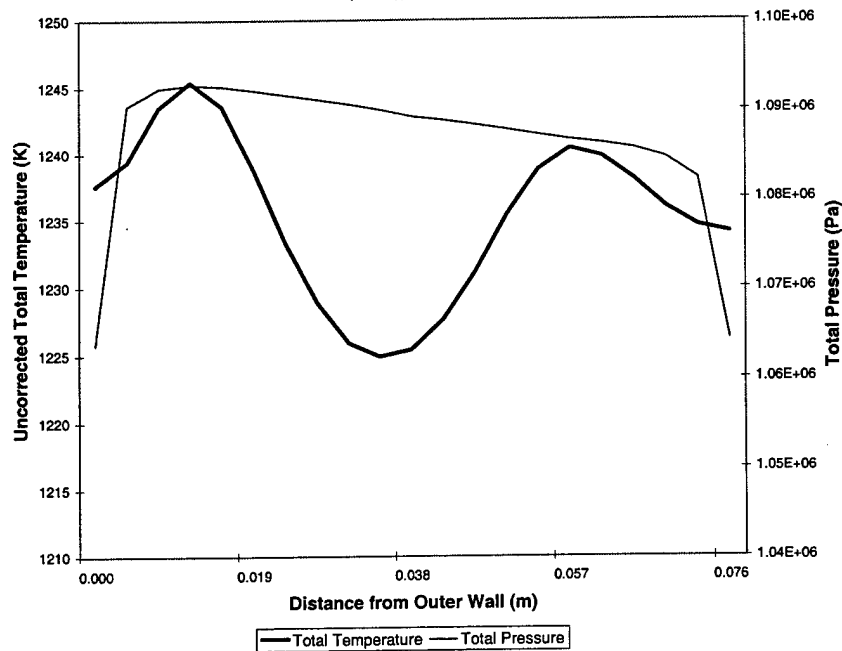


Figure 4.5 Radial Variation of Total Temperature and Total Pressure Across Exit Plane (Location A to Location B in Figure 3.5), Full-Scale Concentric Tube Heat Exchanger, 2.0 mm Thick Tubes

The full-scale concentric tube geometry was also evaluated at three altitudes to establish the ability of the heat exchanger to function over a reasonable flight

envelope. Data from OFFX (23) was used to generate new inlet conditions for the three different cases: 15,000 ft at Mach 0.8; 30,000 ft at Mach 0.8; and 45,000 ft at Mach 0.8. These are found in Table 4.1.

Table 4.1 J-57 Burner or Heat Exchanger Inlet Conditions at Typical Flight Altitudes and Mach Numbers

Altitude	Mach Number	Total Temperature	Total Pressure	Inlet Velocity
0 ft	0	622 K	1.15 MPa	112 m/s
15,000 ft	0.8	625 K	0.97 MPa	104 m/s
30,000 ft	0.8	566 K	0.53 MPa	99 m/s
45,000 ft	0.8	536 K	0.26 MPa	95 m/s

Each set of inlet conditions was evaluated for its effect on (corrected) T_{T4} and π_b . The results are shown in Table 4.2.

Table 4.2 Concentric Tube Heat Exchanger Outlet Conditions with Typical In-Flight Inlet Conditions

Altitude	Mach Number	T_{T4}	P_{T4}	π_b
0 ft	0	1150 K	1.09 MPa	94.5%
15,000 ft	0.8	1152 K	0.93 MPa	95.8%
30,000 ft	0.8	1201 K	0.49 MPa	92.3%
45,000 ft	0.8	1283 K	0.25 MPa	96.1%

4.1.2 Trapezoidal Radial Fin Geometry. The second major geometry evaluated was radially oriented, trapezoidal fins. The intent of this design was to keep the spacing between the fins constant in the radial direction on an annular heat exchanger. For this purpose, the inner radius of the heat exchanger was taken to be 30.48 cm (12 inches) and the outer radius was taken to be 50.8 cm (20 inches). With 385 fins, this leaves 4.5 mm spacing throughout and fins 0.5 mm thick at the inner radius and 3.8 mm thick at the outer radius (see Figures 3.6 and 3.7 for illustrations). Relatively constant heat transfer is expected in the radial direction, along with significantly higher pressure loss at the outer radius, just due to pressure drag on the thicker fins. The total temperature at the outlet was expected to drop with increasing fin thickness, due to the higher mass flow through the channel (since the density

and velocity are held constant across the radial direction, the thicker fins will entail higher mass flow, as they capture a larger area). The flow in this three-dimensional area was approximated with two-dimensional cuts in the transverse direction (see Figures 3.7 and 3.8, size data found in Table 3.1). Data from these cuts was linearly interpolated to form a distribution in the radial direction, and an area weighted average total temperature and pressure were calculated. The distributions are shown in Figure 4.6 for an inlet velocity of 41 m/s and in Figure 4.7 for an inlet velocity of 29 m/s. At 41 m/s inlet velocity, the average T_{T4} is 1106 K (1990°R), or 1040 K (1872°R) corrected, and the average pressure ratio (π_b) is 96.8%, while at 29 m/s inlet velocity, the average T_{T4} is 1212 K (2181°R), 1130 K (2033°R) corrected, and the average π_b is 97.4%. It should be noted that the total pressure and temperature here do not include the diffusion or compression pressure losses of the inlet or outlet manifolds and possible temperature losses due to cooling air injection. From the radial inlet and outlet, the combined estimated pressure ratio of the inlet and outlet is 99.7%. This reduces the total pressure ratio to approximately 96.5% for 41 m/s inlet velocity and 97.1% for 29 m/s inlet velocity, the numbers that were used for thrust calculations. Again, for comparison of average total temperature and total pressure ratio with other geometries, see Table 4.6.

As with the concentric tube geometry, heat transfer coefficients were evaluated to ensure that they stayed within reasonable bounds. The variation of heat flux and heat transfer coefficient along the center of the trapezoidal fin is shown in Figure 4.8. As shown in Figure 4.8, the heat transfer coefficient varied from about 1,000 $\frac{W}{m^2K}$ at the leading edge of the fin, and dropped steadily to about 650 $\frac{W}{m^2K}$ at the trailing edge of the fin. These were well below the prediction of 2,000 $\frac{W}{m^2K}$ derived from Kays and Crawford (9:327). Again, the data matched closely with predictions found in Hill and Peterson (20:129), and since the other cases behaved similarly, the ANSYS® (11) data was taken as a reasonable approximation of reality.

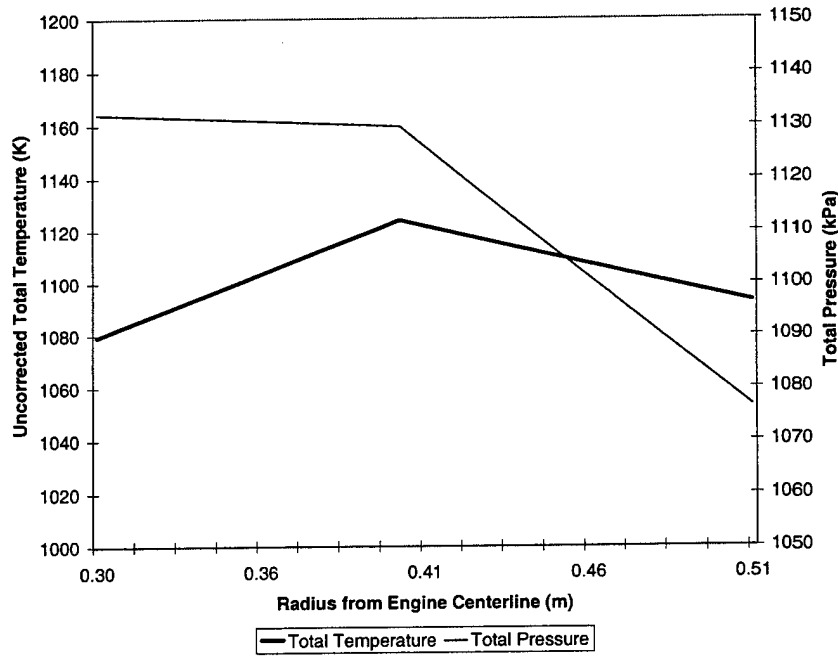


Figure 4.6 Radial Variation of Total Temperature and Total Pressure Across Exit Plane, Trapezoidal Radial Fin Heat Exchanger at 41 m/s Inlet Velocity

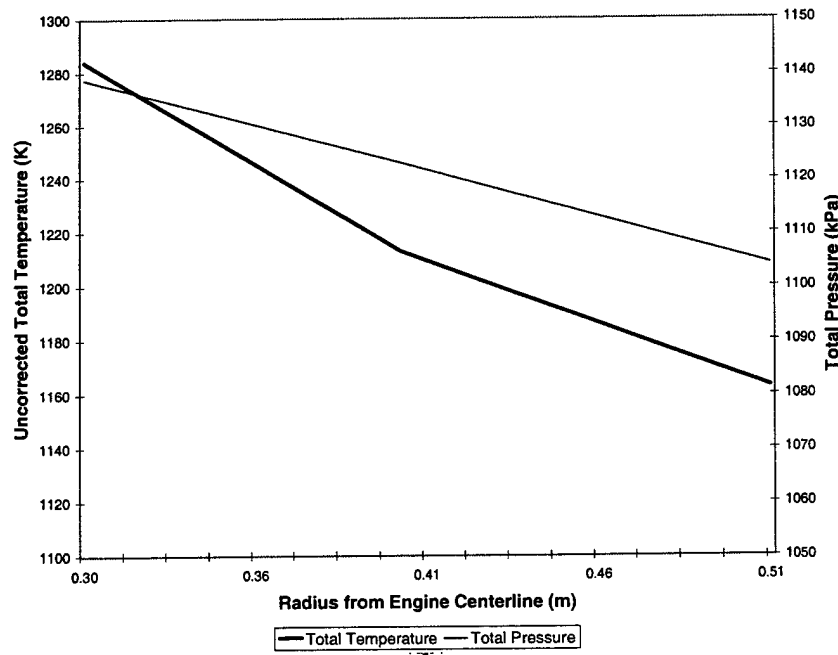


Figure 4.7 Radial Variation of Total Temperature and Total Pressure Across Exit Plane, Trapezoidal Radial Fin Heat Exchanger at 29 m/s Inlet Velocity

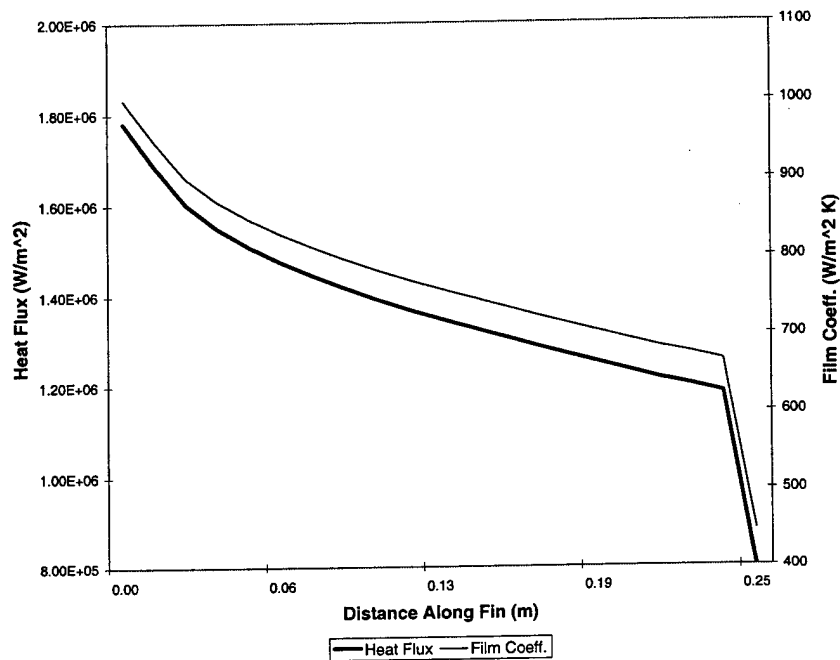


Figure 4.8 Axial Distribution of Heat Flux and Heat Transfer Coefficient at Radial Center of Trapezoidal Radial Fins at 41 m/s Inlet Velocity

4.1.3 Rectangular Radial Fin Geometry. A second option for radial fins was the rectangular fin with variable spacing. This used two annuli of 2 mm thick fins. The inner annulus had an inner radius of 30.48 cm and an outer radius of 40.64 cm. With 344 fins, this gives fin spacing from 3.57 mm to 5.38 mm. The outer annulus had an inner radius of 40.64 cm and an outer radius of 50.8 cm. This allowed 442 fins with spacing from 3.78 mm to 5.22 mm (see Figures 3.8, 3.9, and 3.10 for illustrations of the geometries involved in this case, dimensions can be found in Table 3.2). Each annulus was approximated with three transverse cuts similar to those used for the trapezoidal fins (see Figures 3.8 and 3.10, and Table 3.2) at the inner radius, outer radius, and at 4.5 mm spacing (the middle). The data was linearly interpolated between these cuts and an area-weighted average was calculated from the interpolation. The distribution of total pressure and total temperature is shown in Figure 4.9 for 41 m/s inlet velocity, and in Figure 4.10 for 29 m/s. In both of these distributions there was a noticeable discontinuity in total

temperature and total pressure. This was caused by the transition from the outer edge of the inner annulus to the inner edge of the outer annulus (see Figure 3.9 for a schematic view). At this point the spacing between fins changed from 5.5 mm to 3.8 mm, and the characteristics of the flow change accordingly (total temperature rises and total pressure drops). The average T_{T4} at 41 m/s inlet velocity was 1148 K (2066°R), or 1076 K (1936°R) corrected, and the average pressure ratio (π_b) at 41 m/s inlet velocity was 97.6 %. At 29 m/s inlet velocity, the average T_{T4} was 1221 K (2197°R), 1137 K (2047°R) corrected, and the average π_b was 97.8%. Again, these total pressures and temperatures do not reflect losses in the inlet or outlet manifolds, which would be similar to the estimates for the trapezoidal fins, at 0.3% total pressure loss (to 97.3% for the 41 m/s inlet velocity, and 97.5% for the 29 m/s inlet), and an indeterminate total temperature loss due to cooling air. For comparison of these performance parameters to those for other geometries, see Table 4.6.

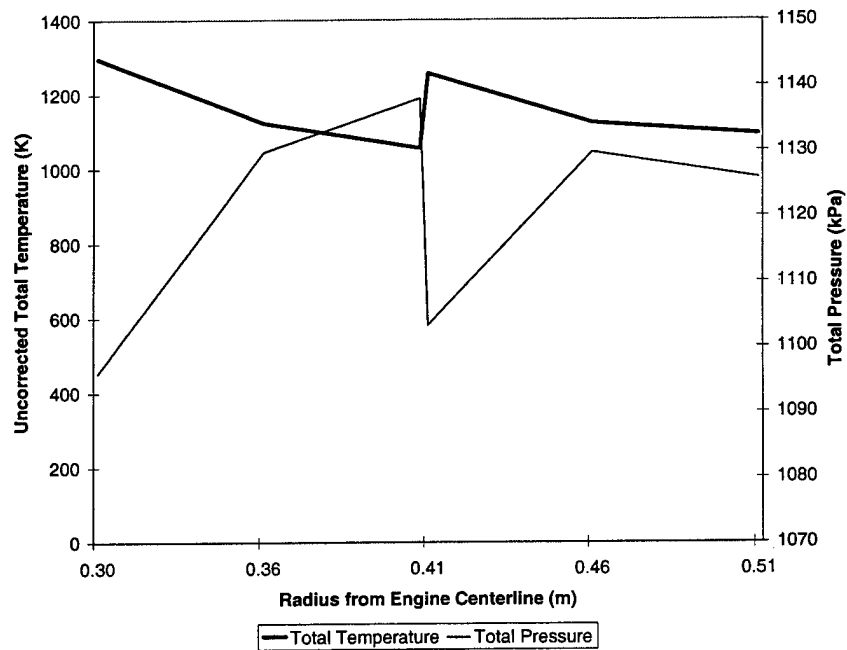


Figure 4.9 Radial Variation of Total Temperature and Total Pressure Across Exit Plane, Rectangular Radial Fin Heat Exchanger at 41 m/s Inlet Velocity

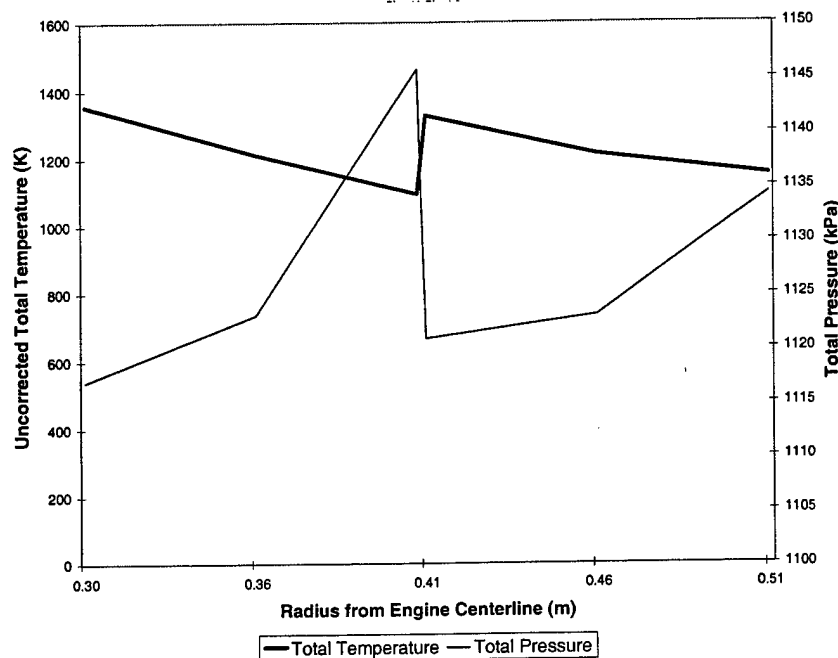


Figure 4.10 Radial Variation of Total Temperature and Total Pressure Across Exit Plane, Rectangular Radial Fin Heat Exchanger at 29 m/s Inlet Velocity

4.2 Heat Exchanger Performance Trends

By recasting some of the data taken for the various geometries, some basic trends could be derived as to which parameters (length, spacing, fin thickness, etc) affected heat exchanger performance, and how significantly. By rearranging the rectangular fin data, one can show a general trend in the performance variation due to fin spacing. As Figure 4.11 shows, increasing fin spacing decreased the total temperature available and increased the total pressure available. However, this was a very small change in total pressure, and a fairly wide variation in total temperature. For comparative purposes, a single run was made with 2.0 mm fins, 4.5 mm spacing, and 508 mm long fins rather than 254 mm fins, while keeping all boundary conditions identical (at 41 m/s inlet velocity). The temperature change across the heat exchanger rose from +433 K (with the shorter fins) to +712 K (with the longer fins)(+779°R to +1282°R), while the pressure loss rose from 1.8% to 3.8%.

By recasting these changes into the form of a L/D_h ratio, and taking the 254 mm length, 9.0 mm D_h as the baseline, it can be shown that a 29% increase in L/D_h leads to a 42% increase in temperature change, and a 100% increase in L/D_h leads to a 66% increase in temperature change. While this shows that changes to fin spacing or fin length would significantly affect the outlet temperatures, the fins cannot be simply made very close and very long to get extremely high outlet temperatures. If the solidity (solidity = $\frac{Volume_{solid}}{Volume_{total}}$) of the heat exchanger is too high, the mass flow through each channel will increase dramatically ($V \propto \frac{1}{1-solidity}$) partially offsetting the temperature gains (for the geometries used here the solidity varies from 30.8% for the dual annulus of rectangular fins, to 32.4% for the trapezoidal fins, with the concentric tubes in between at 31.8%). In addition, Fanno Line flow (isothermal flow in a constant area duct with friction) and Rayleigh Line flow (frictionless flow in a constant area, heated duct) show that there is a limit to the L/D_h ratio that could be used. At some point, from the combination of friction and heat addition, the Mach number will reach 1, at which point the flow can no longer accelerate, and the mass flow must be reduced. The increased temperatures will tend to delay this, but will lead to decreasing total pressure also. This situation would reduce the efficiency of the engine dramatically. In the short heat exchangers used in this research, this situation is not present, but if very high L/D_h ratios were used, this could be a problem.

The data for both the rectangular fins and the trapezoidal fins demonstrate the effect of lowering inlet velocity. The lower velocity impinging on the fins leads to significantly increased outlet temperatures. Again, this is due to the mass flow dropping faster than the heat transfer coefficients. A further demonstration of this effect was seen in the altitude variation data for the full-scale concentric heat exchanger. This data was recast into a variation in Reynolds number based on hydraulic diameter ($Re_{D_h} = \frac{\rho V D_h}{\mu}$). For this comparison the velocity is derived from the mass flow into the burner section of the J-57 at various flight conditions, expanded (in

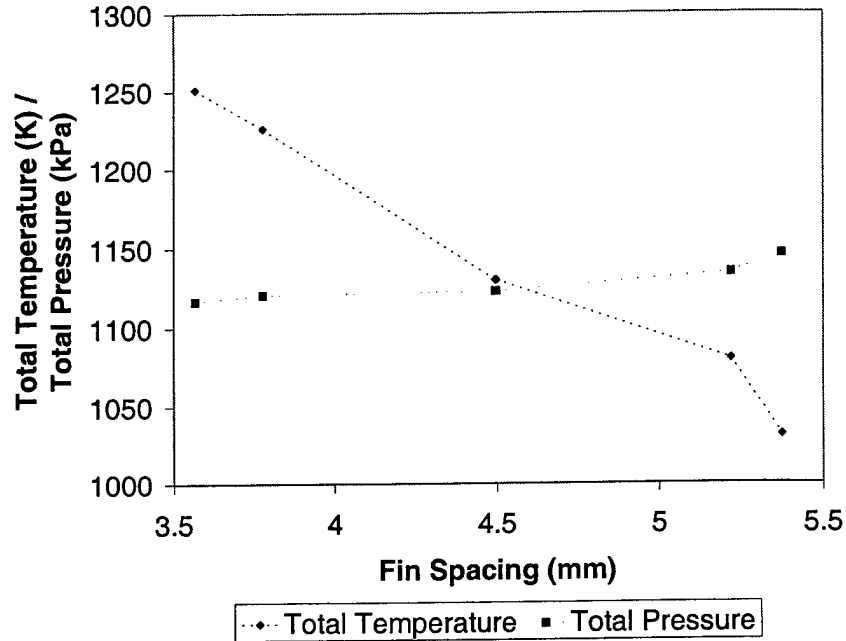


Figure 4.11 Effects of Fin Spacing on Corrected Total Temperature and Pressure at Heat Exchanger Outlet Plane, at 29 m/s Inlet Velocity

a one-dimensional, incompressible calculation) from the compressor exit to an area 4 times greater (this should be, on the average, the velocity just before the fins or tubes begin), the density and viscosity are derived from the total pressure and temperature exiting the compressor, and the hydraulic diameter of the tubes is twice the spacing, of 0.009 m. The effects of Reynolds number on T_{T4} and π_b are shown in Table 4.3 and Figure 4.12.

Table 4.3 Reynolds Number Effects on T_{T4} and π_b

Reynolds Number	T_{T4}	ΔT_T	ΔP_T	π_b
5.26×10^4	1150 K	+528 K	-0.06 MPa	94.5%
4.08×10^4	1152 K	+527 K	-0.04 MPa	95.8%
2.49×10^4	1201 K	+635 K	-0.04 MPa	92.2%
1.29×10^4	1283 K	+747 K	-0.01 MPa	96.1 %

4.2.1 Heat Exchanger Mass. One important parameter for these heat exchangers will be the mass of hafnium contained in them. This will drive the

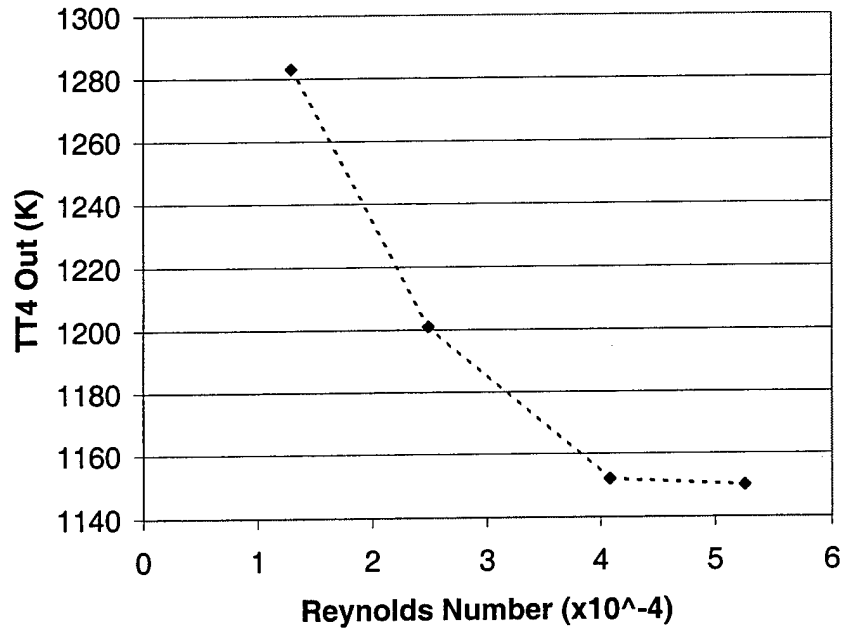


Figure 4.12 Effects of Reynolds Number on T_{T4} Available

endurance available, as well as the structural enhancements required to support the added mass of the heat exchanger in the engine. One area of some uncertainty is the exact density of the hafnium or hafnium alloy as it would be used in the heat exchanger. Therefore, a mass has been calculated for each of the full-scale heat exchangers at the likely extremes of the density range: $13,100 \frac{kg}{m^3}$ and $9,000 \frac{kg}{m^3}$. This data can be found in Table 4.4, and the volume of the fins or tubes is also included. Note that the trapezoidal fin heat exchanger mass is based on solid hafnium fins, although, as described in Section 3.3.10, solid isomer fins are not very realistic for this geometry.

Table 4.4 Mass and Solid Volume of Heat Exchangers

Configuration	Solid Volume	Mass at	
		$\rho = 13,100 \frac{kg}{m^3}$	$\rho = 9,000 \frac{kg}{m^3}$
Concentric Tubes	$0.042 m^3$	549 kg	377 kg
Trapezoidal Fins	$0.043 m^3$	560 kg	386 kg
Rectangular Fins	$0.041 m^3$	531 kg	365 kg

Even on an engine as large as the J-57 (1,757 kg or 3,870 lb), this is a significant addition of mass (365-560 kg). To this we must also add several hundred or thousand pounds of radiation shielding either at the source (the engine) or around sensitive components, or both. This weight gain is offset, though, by the loss of several thousand pounds of fuel weight. These factors would be driven by the application, but it is obvious that the mass increase of the engine will require some significant structural changes. While the exact performance effects of this additional mass cannot be assessed without information about the application, it will not be negligible.

4.3 *Engine Performance Estimates*

4.3.1 *Static Sea-Level Performance.* Performance estimates for the J-57 turbojet with these heat exchangers replacing the conventional combustion chamber were accomplished using the ONX software provided with Mattingly, Heiser, and Daley's book Aircraft Engine Design. This software enables the user to change individual engine parameters to get an on-design thrust estimate for the engine (4:97-133;23).

To evaluate the performance of the J-57 with the heat exchangers in place, it was first necessary to calculate the other parameters for the engine, such as: compressor pressure ratio, compressor and turbine efficiencies, and so forth. These are shown in Table 4.5. By taking these parameters to be fixed, the thrust of the engine can be estimated with the heat exchangers in place by changing T_{T4} and π_b . The results of these calculations are found in Table 4.6. Please note that the pressure ratios for the radial fin geometries include estimated pressure losses for the inlet and outlet manifolds, derived from the radial inlet and outlet models.

All three of the full-size geometries exceeded the thrust value of the conventional J-57 turbojet (10,344 lbT, as calculated using ONX)(23). The reader should note that the higher velocity (41 m/s) runs with the radial fin geometries would

Table 4.5 Critical Engine Parameters for the J-57 Turbojet

Calculated Values	
π_{cl} (Low Pressure Compressor Pressure Ratio)	3.673
π_{ch} (High Pressure Compressor Pressure Ratio)	3.092
η_{cl} (Low Pressure Compressor Polytropic Efficiency)	0.885
η_{ch} (High Pressure Compressor Polytropic Efficiency)	0.923
η_t (Turbine Polytropic Efficiency)	0.938
Assumed Values	
γ_c (Cold Ratio of Specific Heats)	1.4
γ_h (Hot Ratio of Specific Heats)	1.3
$\pi_{D_{max}}$ (Maximum Diffuser Pressure Ratio)	0.97
$\pi_{n_{max}}$ (Maximum Nozzle Pressure Ratio)	0.98
η_{ml} (Mechanical Efficiency, Low Pressure Spool)	0.98
η_{mh} (Mechanical Efficiency, High Pressure Spool)	0.98
Bleed Air Percentage	1.0%
Cooling Air Take-off #1	5.0%
Cooling Air Take-off #2	5.0%
Power Take-off	250 kW
\dot{m} (Engine mass air flow)	167 lbm/s

Table 4.6 Estimated J-57 Sea Level Static Thrust with Heat Exchangers Installed

Heat Exchanger Type	T_{T4}	π_b (K)	Thrust (lbT)	% of J-57
0.5 mm Concentric Tubes	1027 K	96.8%	8,964	86.6%
2.0 mm Concentric Tubes	986 K	97.0%	8,301	80.2%
0.5 mm Staggered Concentric Tubes	1042 K	95.0%	9,105	88.0%
Full-Scale Concentric Tubes	1150 K	94.5%	10,619	102.7%
Trapezoidal Radial Fins (41 m/s)	1040 K	96.5%	9,147	88.4%
Trapezoidal Radial Fins (29 m/s)	1130 K	97.1%	10,488	101.4%
Rectangular Radial Fins (41 m/s)	1076 K	97.3%	9,736	94.1%
Rectangular Radial Fins (29 m/s)	1137 K	97.5%	10,607	102.5%

represent a higher mass flow rate through the heat exchanger. An increased mass flow rate would alter the performance from that listed here, but would not represent the effect of installing these heat exchangers in an off-the-shelf engine. The higher velocity data would also represent the effect of installing a smaller (radially) heat exchanger to accommodate space restrictions. It should also be noted that these static, sea level thrust values only represent part of the overall performance picture. They do not represent the variation in heat exchanger, and engine, performance which would occur due to altitude and off-design operation conditions.

4.3.2 Performance at Other Flight Conditions. From the data for the full-scale concentric tube geometry, the flight performance of the heat exchanger can be seen. The heat exchanger proved capable of heating the flow to higher temperatures at higher altitudes. The J-57, though, cannot use this excess capacity. As the aircraft climbs, the engine needs less total temperature capability to allow the compressor to operate at its limiting pressure ratio. Therefore, as the aircraft climbs, the requirement for turbine inlet temperature drops. This trend is shown in Figure 4.13. Since the heat exchanger proved able to produce more turbine inlet temperature than needed, the requirement could be matched by lowering the average wall temperature until the T_{T4} requirement was met. Under these conditions, the engine with heat exchangers installed should very nearly match the baseline J-57's performance under flight conditions.

4.4 Grid Independence

Due to the size of the concentric models, and the fact that spacing was nearly identical in the radial fin models, grid independence was checked with a radial fin model, with 0.5 mm thick fins and 4.5 mm spacing. The results showed a 1 degree increase in outlet temperature (about a 0.2% change) and a 0.2% increase in outlet total pressure. Therefore, the data was largely grid independent.

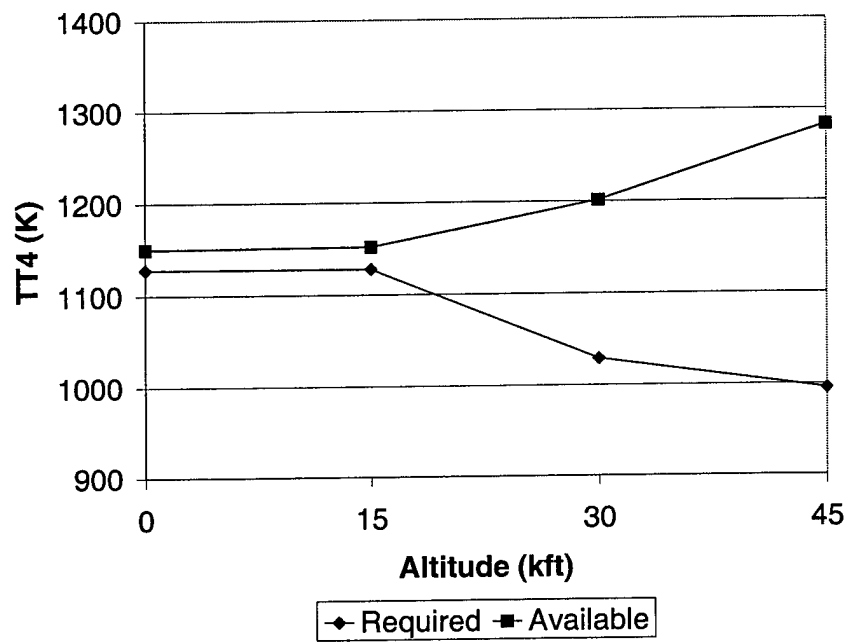


Figure 4.13 Effects of Altitude on Required and Available T_{T4}

V. Conclusions and Recommendations

This chapter contains conclusions based on the current work and recommendations concerning directions for future research in this area.

In this research, three heat exchanger configurations (concentric tubes, radial fins with constant spacing, and radial fins with constant thickness) were evaluated for their performance in a gas-turbine environment. The performance ratings used were the exit total temperature and the total pressure loss. In a gas turbine engine these translate to the turbine inlet temperature, T_{T4} , and burner pressure ratio, π_b . The intended application of this research would be the use of a radioactive isomer whose rapid decay can be triggered and controlled, to power a high endurance jet aircraft. The research was based on the following assumptions: 1) That the decay process can be controlled. 2) That the isomer, and whatever materials it may be alloyed with or contained in, have similar material properties to pure metallic hafnium (especially the melting point). 3) That the heated surfaces of the heat exchanger would be manufactured from the isomer and its associated materials. Assumptions in these areas were necessary to begin analysis, and these were judged reasonable.

Heat exchanger geometries were intended to fit within the envelope of the combustion chamber section of a J-57 turbojet engine. The J-57 was also used as a source for entrance conditions to the heat exchangers, and as a baseline for performance comparisons.

5.1 Conclusions

The following conclusions are presented based on the data in this research, and the entering assumptions.

1. Any of these three configurations, if it can be manufactured, and the heat generation rates can be controlled at a close to uniform level, should be a feasible replacement for the combustion chamber in a turbojet. This feasibility is based only

on the thermodynamics and fluid mechanics of the problem, and does not consider application driven or operational considerations. The manufacturability of these heat exchangers is largely a machining question, and a question of the availability of large quantities of the isomer.

2. Engine operations at higher altitudes should be easier than at sea level. In general, the temperature requirements will be lower, while the capability of the heat exchanger to raise the temperature of the flow is increasing. In addition, the lower mass flow rates at high altitudes will reduce the energy and radiation output of the heat exchanger, extending endurance and limiting the radiation exposure of sensitive components of the aircraft.

3. The extraordinary endurance offered by this heat source could drastically change the operating paradigms for many missions. Overall, this research showed that an isomer heat source may be feasibly harnessed to power a turbojet (or turbofan) engine, if the radiation problem can be dealt with.

5.2 Recommendations

There are several directions that could be taken from this work. Some of these are listed below, in no particular order of precedence.

1. Optimization of the heat exchanger geometry for a given airframe and engine geometry. For example, given hard limits on the turbine inlet temperature and pressure capacity of an engine, design a heat exchanger geometry for maximum thrust, or maximum endurance. Obviously, this would require some knowledge of the proposed mission for the aircraft. An engine design could even be optimized for minimal radiation, which would probably lead to engine designs similar to those for maximum fuel efficiency, with low hot mass flows, and high bypass ratios. To take this path would require some specification of airframe and engine data.

2. Some consideration must be given to aeroelasticity in this heat exchanger. The minimum stiffness of the fins (calculated from the material properties and ge-

ometry) which can be used should be determined. From the material properties for hafnium listed in the ASM Handbook (27:665), this could be quite thin, but this data did not include temperature variations of these properties. Closely related is the resistance to corrosion or erosion of the hafnium in this high-temperature environment with constant airflow, probably carrying particulates of some type. Detailed studies of the material behavior at high temperatures, up to the melting point, may be required.

3. Structural considerations also need to be addressed. Support of this very high temperature, very heavy heat exchanger should be addressed. The use of some type of ceramic supports, separators, or insulators could be evaluated. Air cooling requirements for the structural members of the heat exchanger could be included. These are some of the structural issues which would require analysis before an operational engine could be built.

4. The use of still thicker fins could be evaluated, with the aim of using hollow fins made of some highly refractory material, such as titanium carbide or hafnium carbide, to contain liquid hafnium isomer. This might allow wall temperatures of 3,000 K or even higher. This could allow much higher heat transfer or more compact heat exchangers. Obviously, the chemical reactivity of the hafnium at that point would need to be evaluated, as well as the properties of the fin casing material at extremely high temperatures.

5. Given that the use of this isomer in a gas-turbine engine is feasible, a detailed study of the radiation shielding requirements may be in order. This would probably include: the exact spectrum of radiation emitted by the heat exchanger in full-throttle operation, some determination of the maximum radiation dose permissible to the most sensitive components (the pilot if the aircraft is manned), and, given an airframe geometry (engine location relative to sensitive components) and some material limitations, design radiation shielding to limit radiation exposure to

acceptable level. This area of study is probably best left to physicists or nuclear engineers, who have a background in radiation shielding.

6. Some study could be made of the operational considerations this power source would entail. This could include, but is not limited to: considerations for maintenance personnel who have to work on the engine or aircraft; operational safety considerations including take-off and landing radiation hazards to personnel at the airfield; disposal of used heat exchanger fins; crash safety of the heat exchangers; and political considerations of operating this type of aircraft over populated areas or in foreign airspace. All of these considerations would need to be addressed before this type of system could be operational.

Appendix A. Temperature Corrections for Variable Specific Heats

Since ANSYS® (11) cannot use a variable specific heat with a compressible flow, it was necessary to correct the temperature data at the end of the process.

This correction was based on two premises: first, that the heat transfer data is not significantly affected by the temperature errors introduced by the fixed specific heat; and second; that the variation in specific heats can be adequately represented by the algebraic average of the specific heats at the high and low temperatures in the process. As for the first assumption, the heat transfer coefficients are largely determined by the Reynolds number of the flow at the specific location. Temperature has direct effects on two parts of the Reynolds number: the density and the viscosity. The density, however, is part of a product with velocity. Since the mass flow is constant, therefore, the Reynolds number is unchanged by fluctuations in density. The temperature changes in viscosity are not similarly negated, but are fairly small in the range of the temperature change at any given location in the flow due to the specific heat variation (less than 100 K). For the second assumption, a check of the variation of flow enthalpy with temperature shows that the average specific heats between two points are determined by:

$$c_p = \frac{\Delta h_{1,2}}{\Delta T_{1,2}} \quad (\text{A.1})$$

This is very close (within <1%) to the algebraic average of the c_p for the end points. Therefore the outlet temperatures were corrected using the following method.

Step 1: The enthalpy change is computed from:

$$\Delta h = c_{p_{ANSYS}}(T_{T_{out}} - T_{T_{in}}) \quad (\text{A.2})$$

Step 2: The c_p for the inlet temperature is computed from a correlation found in Wilson and Korakianitis (32:575). This correlation is of the form: $\sum_{i=0}^n C_i T^i$, with C_i given for ranges of temperatures.

Step 3: The c_p for the initial outlet temperature is computed from the appropriate correlation in Wilson and Korakianitis, and an average c_p is calculated.

$$c_{p_{avg}} = \frac{c_{p_{low}} + c_{p_{high}}}{2} \quad (A.3)$$

Step 4: The new outlet temperature is generated from the following equation:

$$T_{T4_{new}} = \frac{\Delta h}{c_{p_{avg}}} + T_{T3} \quad (A.4)$$

Step 5: A new $c_{p_{avg}}$ is computed, based on the new T_{T4} , and the process repeats until a converged value is established.

Appendix B. Building a Model in ANSYS®

This Appendix covers the basics of building a simple heat exchanger model in ANSYS® 5.6.1(Faculty Research Release) (11). These instructions were based on the methods, software, and hardware used in this research. ANSYS® 5.6.1 was run on a 700 MHz Pentium III® PC, with 384 Mb RAM, a 19" monitor, and 2.0 Gb hard drive (if purchasing hardware to run this software, maximize RAM and storage, minimize fluff such as speakers and sound cards. A CD ROM drive is mandatory for installation, large capacity backup drives would be useful.)

Step 1. Start ANSYS®. (in Windows®: PROGRAMS, ANSYS®, INTERACTIVE)

Step 2. Enter Initial Jobname (ex: heatexchanger1), press RUN.(If you specify an existing file, it will open that file. If you do not want to overwrite the old file, you should press RESUME-DB as soon as ANSYS® starts.) This jobname will be the name of all files associated with this model.

Step 3. Go to PREFERENCES, press FLOTRAN® CFD, press OK. This tells ANSYS that you want to run a CFD model. Note that no other types of elements can be present in CFD models.

Step 4. Go to PREPROCESSOR, ELEMENT TYPE, ADD/EDIT/DELETE, ADD, select 2D FLOTRAN® 141, OK, CLOSE. Close ELEMENT TYPE Menu. This tells ANSYS that you will be running a 2-D analysis. Again, only FLOTRAN element types are permitted in a CFD analysis.

Step 5. Go to CREATE Submenu. Select AREA, RECTANGLE, BY DIMENSIONS. Enter the following rectangles:

X1	X2	Y1	Y2
0	0.0254	0.0127	0.0381
0.0762	0.3302	0	0.054
0.381	0.4064	0.0127	0.0381
0.4064	0.75	0.0127	0.0381

This creates the entrance, body, and exit of the heat exchanger. The dimensions are all in meters.

Step 6. Select LINE, LINES, TAN TO 2 LINES, connect the top and bottom of the first rectangle to the top and bottom of the second, and the top and bottom of the second to the top and bottom of the third, following the directions on the screen.

Step 7. Select AREA, ARBITRARY, BY LINES. Select each of the four lines making up the expanding and contracting areas on either side of the second rectangle. This makes these into ANSYS® areas. Steps 6 and 7 create smooth transitions from the inlet to the body and the body to the outlet.

Step 8. Close CREATE menu. Open OPERATE menu, select ADD, AREAS. Select all areas. This makes all six areas into one large area. This completes the envelope of the heat exchanger.

Step 9. Close OPERATE menu. Open CREATE menu. Select AREA, RECTANGLE, BY DIMENSIONS. Create the following rectangles:

X1	X2	Y1	Y2
0.0762	3302	0.0045	0.0055
0.0762	3302	0.01	0.011
0.0762	3302	0.0155	0.0165
0.0762	3302	0.021	0.022
0.0762	3302	0.0265	0.0275
0.0762	3302	0.032	0.033
0.0762	3302	0.0375	0.0385
0.0762	3302	0.043	0.044
0.0762	3302	0.0485	0.0495

This creates the nine fins or tubes of this heat exchanger. Each is 254 mm long and 1 mm thick.

Step 10. Close CREATE menu. Open OPERATE menu. Select SUBTRACT. Select the large envelope area (this is the area we subtract from). Enter. Select the nine small rectangles just created (these will be subtracted). Enter. Now the area of the heat exchanger has nine voids where the fins are, and flow is not allowed. The picture on your screen should look very similar to the compact concentric geometry shown in Chapter 3, Figure 3.2. Close OPERATE menu.

Step 11. Open MESHTOOL. Select LINE-SET. Set all lines to equal spacing at about 0.6 mm per division ($\text{Number of Divisions} = 1.6 \cdot \text{line length in mm}$, all dimensions were entered in m). Select Tri, Free, MESH, Select area on screen, ENTER. ANSYS® will now generate a grid/mesh. Select SAVE-DB at top of screen. The grid should now be present, and will probably be fine enough to meet $y+$ requirements, which we will check later.

Step 12. Open FLOTRAN SET UP. Select settings as follows.

SOLUTION OPTIONS Select: Transient
 Solve Flow Equations

Thermal
 Turbulent
 Compressible
 No for all other options

EXECUTION OPTIONS Select OK (accept Defaults on first menu
 5000 Global Iterations
 Initial time step value = 0
 Number of time steps = 5000
 Global Iterations per time step = 20
 accept all other defaults

ADDITIONAL OUT Select: RFL Out Derived
 YPLU
 TAUW

FLUID PROPERTIES Select: AIR-SI for all properties

FLOW ENVIRONMENT Select: Ref Conditions

REF CONDITIONS Select: Reference Pressure = 1151000 (Pa)
 Ratio of $C_p/C_v = 1.35$
 Nominal Temperature = 622 K
 Total Temperature = 622 K
 Bulk Temperature = 622 K
 Temp offset from absolute zero = 0

CFD SOLVER CONTR Select: VX Solver CFD = TDMA
 VY Solver CFD = TDMA
 TEMP Solver CFD = TDMA
 PRES Solver CFD = PCRS
 ENKE Solver CFD = PGMR
 ENDS Solver CFD = PGMR

TURBULENCE Select: Turbulence Model

Shi-Zhu-Lumley

ADVECTION

Select: Momentum Equations = MSU

Turbulent Equations = SUPG

Compressible Pressure Equations = MSU

Energy Equation = MSU

Most of these entries should be self-explanatory. These will set up ANSYS/Flotran to perform the analysis for a heat exchanger.

Step 13. Open LOADS, APPLY. Apply Constant Temperature to all lines making up the fins (2400). Apply Constant Heat Flux (0) to all other lines, save inlet and outlet. Apply Velocity (X-velocity = 0, Y-velocity = 0) to all lines save inlet and outlet. Apply Velocity (X-velocity = 75, Y-Velocity = 0) to inlet. Apply Pressure DOF (0) to outlet. Apply INITIAL CONDITION, SELECT ALL, VX = 75. Close Loads. Close PREPROCESSOR. Select SAVE-DB. These settings will prohibit flow crossing solid boundaries of the model, impose shear forces along the solid boundaries, impose a heat transfer load on the heated isomer fins of the model, and impose an insulated wall condition on the unheated walls of the model. The 0 (relative) pressure at the outlet is required for subsonic flow, and allows calculation of pressures upstream relative to the outlet condition.

Step 14. Open SOLUTION. Select FLOTRAN® SET UP. Select FLOCHECK, INITIALIZE ALL, ENTER. Select SAVE-DB. This applies the initial conditions and boundary conditions to all of the elements in the model.

Step 15. Select RUN FLOTRAN®.

Step 16. When complete (or Program may be stopped using DONE key on screen), Select SAVE-DB. Close SOLUTION. Open GENERAL POSTPROCES-

SOR. Select READ RESULTS, LAST SET. This enables the postprocessor to use the current solution output to create all of the output displays later.

Step 17. Select PLOT RESULTS, NODAL SOLUTION. This will plot contours of velocity, temperature, pressure, and so forth. Explore these at will. Return to GENERAL POSTPROCESSOR menu. These figures (or any other image in the ANSYS® Graphics window) can be saved through PLOTCTRLS, CAPTURE IMAGE. This will create a bitmap (.BMP) file which can be saved in the filename of choice.

Step 18. Select PATH OPERATIONS. Select DEFINE PATH, BY NODES, Select the top and bottom of the inlet, use 20 divisions, default data sets. Return to PATH OPERATIONS. Select MAP ONTO PATH. Select VX, TEMP, PRES, TTOT, PTOT. Select PLOT PATH ITEM. This will generate plots of the velocity, pressure, etc, along the path. Explore at will. Select LIST PATH ITEM. Select VX, TEMP, PRES, TTOT, PTOT. This will create a listing of the variables and distance along the path specified. The path operations can be repeated for any path desired. Save Path item listings (FILE, SAVE AS), and they can be opened using EXCEL® or some other tool for further analysis.

These instructions should get a new user started. There are many subtleties to using ANSYS®, and only experience will uncover them all. As with any other computer tool, SAVE OFTEN. ANSYS® does consume a significant amount of hard-drive space, so plan accordingly.

Notes:

1. If element counts are above 100,000, runs will be quite slow, and this version of ANSYS® cannot handle over 250,000 elements. A 50,000 element model will occupy about 100 Mb of disk space for model, solution, and associated files.

2. Transient solutions seem more stable than steady-state solutions. It may be possible to run the problem transient for a period and then solve as steady state (not always).

3. Remember that compressible flows must have fixed specific heats. Try to use a good guess at specific heat, and then correct the output if necessary.

4. Remember that all pressure outputs are relative to the reference pressure that was entered in (PREPROCESSOR, FLOTRAN SET UP, FLOW ENVIRONMENT). When using these temperatures in other programs you will need to add the reference pressure back in.

Bibliography

1. Bussard, R.W., and R.D. DeLauer. *Fundamentals of Nuclear Flight*. New York: McGraw-Hill Book Company, 1965.
2. Collins, C.B., F. Davanloo, M.C. Iosif, R. Dussart, J.M. Hicks, S.A. Karamian, C.A. Ur, I.I. Popescu, V.I. Kirischuk, J.J. Carroll, H.E. Roberts, P. McDaniel, and C.E. Crist. "Accelerated Emission of Gamma Rays from the 31-yr Isomer of ^{178}Hf Induced by X-Ray Irradiation," *Physical Review Letters*, 82:695-698 (January 1999).
3. McDaniel, Patrick, AFRL/DEPA. Personal Communication., 2 October 1999.
4. Mattingly, Jack D., William H. Heiser, and Daniel H. Daley. *Aircraft Engine Design*. Washington, D.C.: AIAA Education Series, 1987.
5. Martinez, J.S. "Isotope/Thermal Thrusters and Applications." *Nuclear, Thermal and Electric Rocket Propulsion* edited by R.A. Willaume and A. Jaumotte and R.W. Bussard, New York: Gordon and Breach Science Publishers, 1967.
6. Rom, F.E. "Fast and Moderated Reactors and Applications of Low-Power Nuclear Rockets." *Nuclear, Thermal and Electric Rocket Propulsion* edited by R.A. Willaume and A. Jaumotte and R.W. Bussard, New York: Gordon and Breach Science Publishers, 1967.
7. Bergles, A.E. "Augmented Heat Exchangers for High Temperature Applications." *High Temperature Heat Exchangers* edited by Y. Mori and A.E. Sheindlin and N.H. Afgan, Washington, D.C.: Hemisphere Publishing Company, 1986.
8. Hasegawa, Shu, Kenji Fukada, and Ryoza Echigo. "Improvement of High Temperature Heat Exchanger Efficiency by Inserted Wire Net Layers." *High Temperature Heat Exchangers* edited by Y. Mori and A.E. Sheindlin and N.H. Afgan, Washington, D.C.: Hemisphere Publishing Company, 1986.
9. Kays, W.M., and M.E. Crawford. *Convective Heat and Mass Transfer* (Third Edition). New York: McGraw-Hill Inc., 1993.
10. McEligot, Donald. "Basic Thermofluidynamic Problems in High Temperature Heat Exchangers." *High Temperature Heat Exchangers* edited by Y. Mori and A.E. Sheindlin and N.H. Afgan, Washington, D.C.: Hemisphere Publishing Company, 1986.
11. ANSYS, Inc. *ANSYS Multiphysics*. Finite Element Software Version 5.6.1. Southpointe, Canonsburg, PA (1-800-937-3321), 1999.
12. White, Frank M. *Viscous Fluid Flow* (Second Edition). New York: McGraw-Hill, 1991.

13. Wolff, J. Mitch, and Paul D. Orkwis. Class Handout distributed in AERO 751, Introduction to Numerical Methods in Fluid Mechanics. Graduate School of Engineering and Management, Air Force Institute of Technology (AETC), Wright-Patterson AFB OH, September 1999.
14. Kutateladze, S.S., and A.I. Leontiev. *Heat Transfer, Mass Transfer and Friction in Turbulent Boundary layers*. New York: Hemisphere Publishing Company, 1985.
15. Tannehill, J.C., D.A. Anderson, and R.H. Pletcher. *Computational Fluid Mechanics and Heat Transfer* (Second Edition). Washington, D.C.: Taylor & Francis, 1997.
16. Jones, W.P., and B.E. Launder. "The Calculation of Low-Reynolds Number Phenomena with a Two-Equation Model of Turbulence," *Journal of Heat and Mass Transfer*, 16:1119-1130 (September 1973).
17. Launder, B.E., and D.B. Spalding. "The Numerical Computation of Turbulent Flows," *Computer Methods in Applied Mechanics and Engineering*, 3:269-289 (September 1974).
18. Tennekes, H., and J.L. Lumley. *A First Course in Turbulence*. Cambridge, Massachusetts: The MIT Press, 1972.
19. Shih, Tsan-Hsing, Jiang Zhu, and John L. Lumley. "A new Reynolds stress algebraic equation model," *Computer Methods in Applied Mechanics and Engineering*, 125:287-302 (September 1995).
20. Hill, Phillip, and Carl Peterson. *Mechanics and Thermodynamics of Propulsion* (Second Edition). Reading, Massachusetts: Addison-Wesley Publishing Company, 1991.
21. John, James E.A. *Gas Dynamics* (Second Edition). Boston: Allyn and Bacon, Inc., 1984.
22. Saad, Michel A. *Compressible Fluid Flow* (Second Edition). Englewood Cliffs, New Jersey: Prentice Hall, 1993.
23. Mattingly, Jack D., "ONX and OFFX Software, Version 2.2." Provided with *Aircraft Engine Design* AIAA Education Series, 1996.
24. McDaniel, Patrick, AFRL/DEPA. Personal Communication., 8 December 2000.
25. Turner, James E. *Atoms, Radiation, and Radiation Protection* (Second Edition). New York: John Wiley & Sons, Inc., 1995.
26. ANSYS, Inc. *ANSYS Theory Reference*. User Reference Manual Version 5.6. Southpointe, Canonsburg, PA (1-800-937-3321), 1999.

27. ASM. *Metals Handbook Volume 2 - Properties and Selection: Nonferrous Alloys and Special Purpose Materials* (Tenth Edition). New York: ASM International, 1990.
28. ANSYS, Inc. *ANSYS CFD Flotran Analysis Guide*. Software User's Guide for ANSYS/Flotran Version 5.6.1. Southpointe, Canonsburg, PA (1-800-937-3321), 1999.
29. Gunston, Bill. "Pratt & Whitney JT3." *Jane's Aero-Engines*, (Seventh Edition) edited by Bill Gunston, Coulsdon, Surrey, UK: Jane's Information Group Limited, 2000.
30. Jarcy, Capt Jerome R. *Flow Field, Drag and Heat Transfer of a Heated Cylinder in a Subsonic Crossflow of Air*. MS thesis, AFIT/GAM/ME/67-10, Air Force Institute of Technology, Wright-Patterson AFB OH, June 1967 (AD-818693).
31. Zukauskas, A., and J. Ziugzda. *Heat Transfer of a Cylinder in Crossflow*. New York: Hemisphere Publishing Company, 1985.
32. Wilson, David Gordon, and Theodosios Korakianitis. *The Design of High-Efficiency Turbomachinery and Gas Turbines* (Second Edition). Upper Saddle River, New Jersey: Prentice Hall, 1998.

Vita

Captain Carl R. Hartsfield graduated from Seminole High School in Seminole, Florida in June 1987. He attended the Georgia Institute of Technology, in Atlanta, Georgia, on Reserve Officer Training Corps scholarship. In September, 1991 he graduated with a Bachelor of Aerospace Engineering degree, and was commissioned through Detachment 165, AFROTC.

In 1994, Carl was married, and he and his wife have two daughters.

Captain Hartsfield has had assignments to Kunsan AB, Republic of Korea; Minot AFB, North Dakota; and Wright-Patterson AFB, Ohio. The Air Force Institute of Technology is his fourth assignment. Upon graduation, he will be assigned to the Air Vehicles Directorate, Air Force Research Laboratory, Wright-Patterson Air Force Base, Ohio.

REPORT DOCUMENTATION PAGE

Form Approved
OMB No. 0704-0188

Public reporting burden for this collection of information is estimated to average 1 hour per response, including the time for reviewing instructions, searching existing data sources, gathering and maintaining the data needed, and completing and reviewing this collection of information. Send comments regarding this burden estimate or any other aspect of this collection of information, including suggestions for reducing this burden to Department of Defense, Washington Headquarters Services, Directorate for Information Operations and Reports (0704-0188), 1215 Jefferson Davis Highway, Suite 1204, Arlington, VA 22202-4302. Respondents should be aware that notwithstanding any other provision of law, no person shall be subject to any penalty for failing to comply with a collection of information if it does not display a currently valid OMB control number. PLEASE DO NOT RETURN YOUR FORM TO THE ABOVE ADDRESS.

1. REPORT DATE (DD-MM-YYYY) 08-03-2001	2. REPORT TYPE Thesis	3. DATES COVERED (From - To) Mar 2000 - Mar 2001
--	---------------------------------	--

ANALYSIS OF THE APPLICATION OF A TRIGGERED ISOMER HEAT EXCHANGER AS A REPLACEMENT FOR THE COMBUSTION CHAMBER IN AN OFF-THE-SHELF TURBOJET	5a. CONTRACT NUMBER
	5b. GRANT NUMBER
	5c. PROGRAM ELEMENT NUMBER

6. AUTHOR(S) Carl R. Hartsfield, Captain, USAF	5d. PROJECT NUMBER
	5e. TASK NUMBER
	5f. WORK UNIT NUMBER

7. PERFORMING ORGANIZATION NAME(S) AND ADDRESS(ES) Air Force Institute of Technology Graduate School of Engineering and Management (AFIT/ENY) 2920 P St Bldg 640 WPAFB OH 45433-7765	8. PERFORMING ORGANIZATION REPORT NUMBER AFIT/GAE/ENY/01M-04
---	--

9. SPONSORING / MONITORING AGENCY NAME(S) AND ADDRESS(ES) AFRL/DEPA Attn: Patrick McDaniel 3550 Aberdeen Ave. SE Kirtland AFB, NM 87117-5776	10. SPONSOR/MONITOR'S ACRONYM(S)
	11. SPONSOR/MONITOR'S REPORT NUMBER(S)

12. DISTRIBUTION / AVAILABILITY STATEMENT
Approved for Public Release; Distribution Unlimited

13. SUPPLEMENTARY NOTES

14. ABSTRACT
The objective of this research was to evaluate the feasibility of using the triggered decay of a radioactive isomer in a solid-state heat exchanger to power a gas turbine engine. Primary performance measures were stagnation temperature increase and stagnation pressure drop across the heat exchanger. Analysis was performed using commercial software, and explored three types of heat exchanger: concentric tubes, radial fins with constant spacing, and radial fins with constant thickness. All met or exceeded performance of the baseline J-57 turbojet engine at static sea level conditions. A single configuration of heat exchanger, using concentric tubes, was evaluated at typical in-flight conditions, up to 45,000 ft and Mach 0.8. At every flight condition, the heat exchanger was capable of delivering higher turbine inlet temperatures than the engine required for full-throttle operation at that flight condition. Performance trends in heat exchanger design were evaluated as they affected this application.

15. SUBJECT TERMS
AIRCRAFT NUCLEAR PROPULSION, COMPUTATIONAL FLUID DYNAMICS, HEAT TRANSFER, JET PROPULSION, TURBOJET ENGINES

16. SECURITY CLASSIFICATION OF:			17. LIMITATION OF ABSTRACT UU	18. NUMBER OF PAGES 92	19a. NAME OF RESPONSIBLE PERSON Dr. Paul I. King
a. REPORT U	b. ABSTRACT U	c. THIS PAGE U			19b. TELEPHONE NUMBER (include area code) (937) 255-6565 x 4628